



**INDC(NDS)-0872**  
**Distr. AL+G+NC**

# **INDC International Nuclear Data Committee**

Summary Report of the 2nd RCM of the CRP on

## **Updating Fission Yield Data for Applications**

IAEA Headquarters  
Vienna, Austria  
19-23 December 2022

Ramona Vogt  
Lawrence Livermore National Laboratory  
Livermore, CA, USA  
University of California, Davis  
Davis, CA, USA

Amy Lovell  
Los Alamos National Laboratory  
Los Alamos, NM, USA

Anabella Tudora  
Bucharest University  
Bucharest-Magurele, Romania

Toshihiko Kawano  
Los Alamos National Laboratory  
Los Alamos, NM, USA

Roberto Capote Noy  
IAEA Nuclear Data Section  
Vienna, Austria

May 2024

Selected INDC documents may be downloaded in electronic form  
from <http://nds.iaea.org/publications>  
or sent as an e-mail attachment.

Requests for hardcopy or e-mail transmittal should be directed to  
[NDS.Contact-Point@iaea.org](mailto:NDS.Contact-Point@iaea.org)

or to:

Nuclear Data Section  
International Atomic Energy Agency  
Vienna International Centre  
PO Box 100  
1400 Vienna  
Austria

## Summary Report of the 2nd RCM of the CRP on

# Updating Fission Yield Data for Applications

IAEA Headquarters  
Vienna, Austria  
19-23 December 2022

Ramona Vogt  
Lawrence Livermore National Laboratory  
Livermore, CA, USA  
University of California, Davis  
Davis, CA, USA

Amy Lovell  
Los Alamos National Laboratory  
Los Alamos, NM, USA

Anabella Tudora  
Bucharest University  
Bucharest-Magurele, Romania

Toshihiko Kawano  
Los Alamos National Laboratory  
Los Alamos, NM, USA

Roberto Capote Noy  
IAEA Nuclear Data Section  
Vienna, Austria

### ABSTRACT

The Second Research Coordination Meeting of the IAEA Coordinated Research Project (CRP) on Updating Fission Yield Data for Applications was held in Vienna at the IAEA headquarters from 19 to 23 December 2022, with 23 international experts attending the meeting. The CRP is devoted to evaluation efforts of cumulative and independent fission yields for incident energies from the thermal point up to 14 MeV on actinide targets. Produced fission yield evaluations should include full uncertainty quantification and are expected to combine available experimental data and state-of-the-art model information. The activities undertaken within this CRP were reviewed including the assessment of newly measured data and ongoing evaluation efforts. Technical discussions and the resulting further work plan of this CRP are summarized in this report. The meeting presentations are available at:

[https://www-nds.iaea.org/index-meeting-crp/2RCM\\_FY/index.htm](https://www-nds.iaea.org/index-meeting-crp/2RCM_FY/index.htm).

May 2024



## Contents

1.	INTRODUCTION .....	1
2.	PRESENTATION SUMMARIES.....	1
2.1	New fission product yield experimental data, O. Serot.....	1
2.2	Mass yields evaluation of $^{239}\text{Pu}(n_{\text{th}},f)$ : preliminary results, O. Serot, G. Kessedjian, S.-M. Cheikh, A. Chebboubi .....	3
2.3	Impact of pre-neutron FY data on post-neutron FYs using the FIFRELIN de-excitation code, O. Serot, V. Piau, O. Litaize, A. Chebboubi, G. Kessedjian, S. Oberstedt, A. Oberstedt, A. Göök..	4
2.4	New FY evaluation methodology for JEFF-4.0 and Post-JEFF-4.0, G. Kessedjian, S.M. Cheikh, O. Serot, A. Chebboubi, D. Bernard, V. Vallet, R. Mills, L. Capponi .....	6
2.4.1	New methodology for FY evaluation .....	6
2.4.2	Status of the $^{235}\text{U}(n_{\text{th}},f)$ FY evaluation for JEFF-4T2: tests and validation .....	6
2.5	New experimental data on $^{235}\text{U}(n_{\text{th}},f)$ mass yields using the Lohengrin mass spectrometer (preliminary), G. Kessedjian .....	8
2.6	Preliminary results of $^{252}\text{Cf}$ spontaneous fission isotopic yields via mass measurements at the FRS Ion Catcher, I. Mardor, T. Dickel .....	9
2.7	Progress in experiment, theory and evaluation of fission yields at CNDC, N Shu, S. Liu, Y. Chen, L. Liu .....	10
2.8	Fission yield compilation status, B. Prytichenko.....	12
2.9	I. Influence of energy partition in fission and pre-neutron fragment distributions on independent FPYs ( $Y(Z,Ap)$ , $Y(Ap)$ ) and on kinetic energy distributions of post-neutron fragments. II. Correlation between the excitation energy of pre-neutron fragments and the kinetic energy of post-neutron fragments. Application for $^{235}\text{U}(n_{\text{th}},f)$ , A. Tudora .....	13
2.10	Report on the results of the modeling subgroup, F. Minato .....	14
2.11	Developing the 4D-Langevin model-based fission fragment distribution database for TALYS, S. Chiba .....	15
2.12	Use of TALYS to calculate fission yields and neutron and gamma emission, A. Koning.....	16
2.13	Microscopic determination of fission fragment distributions: current status, S. Hilaire, J.F. Lemaitre .....	17
2.14	Fragment spin properties from FREYA, R. Vogt, J. Randrup .....	18
2.15	Change in reactivity in a PWR pin-cell depletion benchmark using recent FY evaluations, O. Cabellos .....	20
2.16	Progress on UKFY3.7 development, R. Mills.....	22
2.17	Evaluation of fission fragment yields and parameter optimization in CCONE code system, F. Minato.....	23
2.18	The ENDF re-evaluation of FPYs, A. Lovell .....	24
2.19	Preliminary study on photo-nuclear fission product yield evaluation, T. Kawano.....	25
2.20	Verification of the energy dependence of the fission product yields from the GEF code for neutron induced fission of $^{235}\text{U}$ based on delayed neutron temporal data, V.M. Piksaikin.....	25
2.20.1	Introduction.....	25
2.20.2	Experimental set-up .....	26
2.20.3	The measurement procedure and processing of the experimental data.....	29
2.20.4	Results and discussion .....	30

2.21	Benchmarking fission yields with beta decay data (and vice versa), A. Algora .....	32
2.22	Accuracy evaluation of available fission yield data and updating, N. Mohamed .....	35
2.23	Fission Yield data plotter at <a href="https://nds.iaea.org/dataexplorer">https://nds.iaea.org/dataexplorer</a> , S. Okumura .....	35
3.	RECOMMENDATIONS .....	36
APPENDIX 1 – Agenda.....		37
APPENDIX 2 – List of participants .....		39
APPENDIX 3 – Meeting photo.....		41

# 1. INTRODUCTION

The Second Research Coordination Meeting of the IAEA Coordinated Research Project (CRP) on Updating Fission Yield Data for Applications was held in Vienna at the IAEA headquarters from 19 to 23 December 2022, with 23 international experts from CRP participating institutes in twelve member states attending the meeting.

The meeting was opened with a welcome address by the Head of the IAEA Nuclear Data Section, A. Koning, and introduction by the Scientific Secretary of the meeting, R. Capote. R. Mills (UKAEA) was elected Chairperson. A. Tudora (University of Bucharest), A. Lovell (LANL), R. Vogt (LLNL) and T. Kawano (LANL) were elected rapporteurs for each day of the meeting, respectively.

R. Capote (IAEA) briefly introduced the CRP, summarized the objectives, goals, expected deliverables, and timeline, and he stressed that this CRP was devoted to evaluation efforts of cumulative and independent fission yields for incident energies from the thermal point up to 14 MeV on actinide targets. Produced fission yield evaluations should include full uncertainty quantification and are expected to combine available experimental data and state-of-the-art model information.

Fission product yield (FPY) evaluations require both experimental data and theoretical efforts. Measurements often do not cover the entire mass and energy ranges of interest. Thus, theoretical models can fill gaps to complete evaluations. One focus, the priority of evaluating fission yield data for neutron-induced reactions on major actinides, was highlighted by R. Capote. The meeting continued Monday through Thursday with presentations by the participants, followed by extensive discussions. The daily meeting time was constrained by the hybrid nature of the meeting and limited online time due to the wide range of time zones involved. Friday was reserved for more detailed discussions and for the assignment of tasks.

The meeting presentations are available at:

[https://www-nds.iaea.org/index-meeting-crp/2RCM\\_FY/index.htm](https://www-nds.iaea.org/index-meeting-crp/2RCM_FY/index.htm).

## 2. PRESENTATION SUMMARIES

Brief summaries of participants' presentations are given in the following. For the full presentations please refer to the hyperlink above.

### 2.1 New fission product yield experimental data, O. Serot

The purpose of this presentation is to point out the existence of new experimental data on fission product yields that could be useful for this CRP and that are not yet included in the EXFOR database, either because these data are very recent or because the results are still preliminary. The experimental data mentioned here are not exhaustive. They are mainly based on the presentations given at the Nuclear Data for Science and Technology conference in July 2022 (ND-2022) (see Ref. [1]).

#### **The TUNL-LANL-LLNL FPY Collaboration**

A collaboration between Los Alamos National Laboratory (LANL), Lawrence Livermore National Laboratory (LLNL) and the Triangle Universities Nuclear Laboratory (TUNL) was formed to measure the energy dependence of FPY for three main neutron induced fission reactions:  $^{235}\text{U}(n,f)$ ,  $^{238}\text{U}(n,f)$  and  $^{239}\text{Pu}(n,f)$ . The measurements were carried out at TUNL, thanks to the 10 MV Tandem Van de Graaff accelerator that produces monoenergetic neutrons with energies between 0.6 MeV to 14.8 MeV [2]. Three new measurement campaigns from this collaboration presented at the ND2022 are worth noting.

- ***Fission Product Yields from Neutron-Induced Fission of Major Actinides at 6.5 MeV*** [3]  
New cumulative FPYs were determined for the  $^{238}\text{U}(n,f)$  reaction at the incident neutron energy of 6.5 MeV. Activation techniques were used: after irradiation of about one hour, the sample is transported to the HPGe detector where  $\gamma$ -counting occurs. The uncertainties are dominated by

statistics and by gamma ray intensity. Note that rather good agreement with GEF predictions is observed.

- **Short-lived Fission Products from Neutron-Induced Fission of  $^{235}\text{U}$  and  $^{238}\text{U}$  [4]**  
Using the rapid belt-driven irradiated target transfer system (RABITTS) available at TUNL, short-lived FPYs with half-lives from seconds to minutes have been measured. This measurement campaign completes previous FPY measurements with half-lives greater than one hour. Preliminary results for neutron-induced fission of  $^{235}\text{U}$  and  $^{238}\text{U}$  at  $E_n = 4.6$  and  $14.8$  MeV were presented.
- **Fission product yields from photon-induced fission of  $^{240}\text{Pu}$  and neutron induced fission of  $^{239}\text{Pu}$  as a function of incident energy [5]**  
Various cumulative Fission Product yields were measured for two different reactions,  $^{240}\text{Pu}(\gamma, f)$  at  $E_\gamma = 8$  MeV and  $^{239}\text{Pu}(n, f)$  at  $E_n = 1.37$  MeV. In this way, yields from the same compound nucleus ( $^{240}\text{Pu}$ ) with the same excitation energy ( $E^* = 8$  MeV), but different spin distributions can be compared. For both reactions, similar yields were found, confirming the Bohr hypothesis and showing the low impact of the compound nucleus spin on fission yields. Two other excitation energies ( $E^* = 11.2$  and  $15.6$  MeV) were investigated as well.

Lastly, A. Tonchev [6] presented an overview of the experimental results obtained since the beginning of the TUNL-LANL-LLNL collaboration.

- **Measurements on Lohengrin mass spectrometer [7]**  
In a collaboration between the CEA-Cadarache, the LPSC and the ILL, new experimental data on  $^{235}\text{U}(n_{th}, f)$  mass yields were measured using the Lohengrin mass spectrometer. Preliminary results are presented by G. Kessedjian in the present report.
- **$^{252}\text{Cf}$  Spontaneous Fission Yields at the FRS Ion Catcher [8]**  
New independent isotopic fission yields of  $^{252}\text{Cf}$  spontaneous fission were measured at the FRS Ion Catcher (GSI, Germany) in the very asymmetric heavy mass region for  $56 < Z < 63$ . Preliminary results show good agreement with data from the literature.
- **Measurement of Independent Fission Product Yields with SPIDER [9]**  
The upgraded Spectrometer for Ion Determination in fission Research (SPIDER), developed at Los Alamos Neutron Science Center for measuring fission product yields with the 2E-2v method, was used to study  $^{252}\text{Cf}$  spontaneous fission [8]. In the near future, SPIDER will be able to provide fission product yields for (n,f) reactions at various incident neutron energies (from thermal up to 20 MeV).

#### References:

- [1] <https://indico.frib.msu.edu/event/52/contributions/>
- [2] M.E. Gooden, et al., Nucl. Data Sheets **131** (2016) 319.
- [3] R. Malone, et al., <https://indico.frib.msu.edu/event/52/contributions/617/>
- [4] A. Ramirez, et al., <https://indico.frib.msu.edu/event/52/contributions/633/>
- [5] J.A. Silano, et al., <https://indico.frib.msu.edu/event/52/contributions/634/>
- [6] A. Tonchev, et al., <https://indico.frib.msu.edu/event/52/contributions/621/>
- [7] G. Kessedjian, et al., Summary 2.5, present report
- [8] Y. Waschitz, et al., <https://indico.frib.msu.edu/event/52/contributions/620/>; EPJ Web Conf. **284** (2023) 04005.
- [9] P. Gastis, et al., <https://indico.frib.msu.edu/event/52/contributions/618/>

#### Q & A, Comments (C)

C: It is not surprising that TUNL (n,f) and ( $\gamma$ ,f) results give the same cumulative FPYs for equivalent excitation energies.

C: SPIDER will include TKE measurements; starting with  $^{252}\text{Cf}$  (as calibration) and then including neutron-induced fission. Data will likely be finalized outside of the CRP timeframe but useful in the future.



Q: Has the LLNL data been published yet? Few marked as in press possibly, but it doesn't sound like there are e.g. Phys. Rev. papers.

A: R. Vogt checked whether ND2022 conference proceedings were submitted by the TUNL-LANL-LLNL teams. They were not. The data are preliminary but they are still working on (target mass) corrections so the work probably won't be published until those results are finalized

Q: Can SPIDER be used to measure the charge distribution with the  $2E-2\nu$  method?

A: This is possible only for the light peak – it depends on the resolution of the ionization chamber.

## 2.2 Mass yields evaluation of $^{239}\text{Pu}(n_{\text{th}},f)$ : preliminary results, O. Serot, G. Kessedjian, S.-M. Cheikh, A. Chebboubi

Preliminary results of mass yields evaluation for  $^{239}\text{Pu}(n_{\text{th}},f)$  are presented. The first step of this work is to make a selection of the experimental data available in the EXFOR database [1]. Fourteen datasets were selected: Six datasets correspond to measurements performed on the Lohengrin mass spectrometer and 8 datasets correspond to cumulative fission yields measured by chemical separation of the fission products. Hence, 228 experimental data points covering the mass range  $68 < A < 154$  were considered (see Fig. 1), covering 83 masses since four masses are not measured ( $A = 115, 121, 123$  and  $153$ ). With this selection, both peaks are almost entirely covered, allowing absolute normalization of the evaluation.

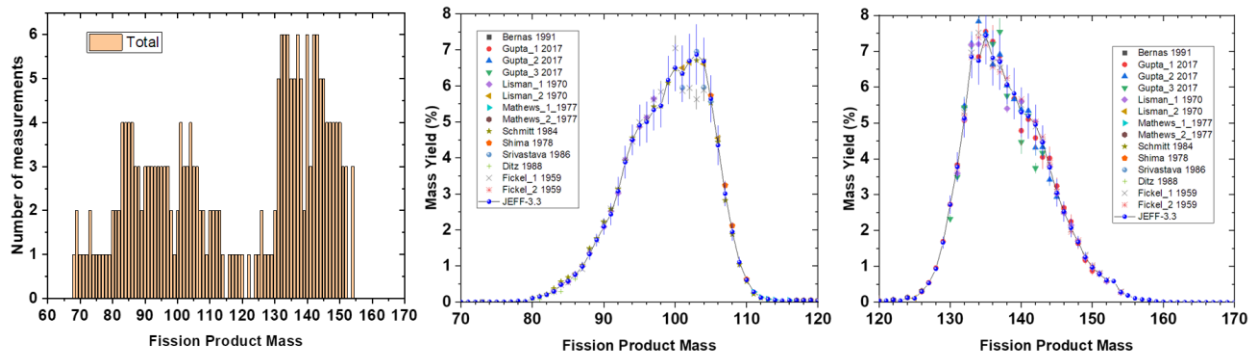


Fig. 1. Left: The number of measurements considered for the  $^{239}\text{Pu}(n_{\text{th}},f)$  mass yield evaluation. Middle: experimental data selected in the light mass region, compared to the JEFF-3.3 evaluation. Right: experimental data selected in the heavy mass region, compared to the JEFF-3.3 evaluation.

The mass yield evaluation is based on the methodology described in Refs. [2-3]. Based on a compatibility test between all the datasets, two mass yield evaluations are proposed, both of which are model independent:

- A “conservative” evaluation, where additional uncorrelated uncertainties (3%) were applied to experimental data in order to make them compatible with each other, therefore keeping as much experimental data as possible.
- A “strict” evaluation, where experimental uncertainties are unmodified, leading to the exclusion of data that are not compatible with each other (11 experimental data were rejected to obtain an acceptable  $\chi^2$ ).

The “strict” evaluation is very close to the JEFF-3.3 evaluation except for some masses in the heavy mass region (left and middle sections of Fig. 2). By construction, uncertainties for the “conservative” evaluation are higher than those of the “strict” evaluation. Note that the uncertainties of the “strict” evaluation are compatible with the experimental uncertainties obtained employing the Lohengrin spectrometer [4]: around 2% in the light mass peak, a little larger near the heavy mass peak (right side of Fig. 2). Both solutions have similar covariance matrices which arise primarily from the normalization and mass and charge conservation.

The last step, still ongoing, involves building isotopic and isomeric yield evaluations by combining the mass yield evaluation with JEFF-3.3, as done for the  $^{235}\text{U}(n_{\text{th}},f)$  fission yields.

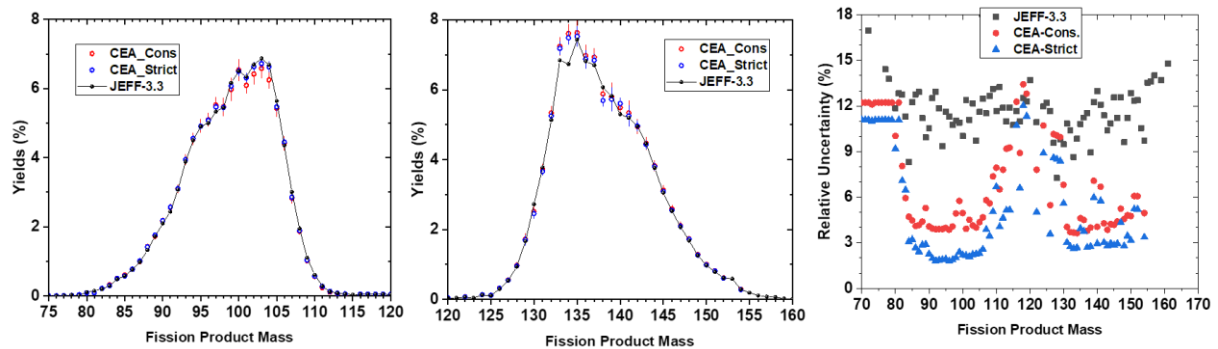


Fig. 2. Comparison of the two proposed mass yield evaluations (“strict” and “conservative”) with that of the JEFF-3.3 library (preliminary results). Left: light mass yields. Middle: heavy mass yields. Right: relative uncertainties over the full mass range.

#### References:

- [1] <https://www-nds.iaea.org/exfor/>
- [2] S.M. Cheikh, PhD thesis, University of Grenoble Alpes, France (2023).
- [3] S.M. Cheikh, G. Kessedjian, O. Serot, et al., EPJ Web Conf. **284** (2023) 08002.
- [4] A. Chebboubi, G. Kessedjian, O. Serot, et al., Eur. Phys. J. A **57** (2021) 335.

### 2.3 Impact of pre-neutron FY data on post-neutron FYs using the FIFRELIN de-excitation code, O. Serot, V. Piau, O. Litaize, A. Chebboubi, G. Kessedjian, S. Oberstedt, A. Oberstedt, A. Göök

FIFRELIN (FISSION FRAGMENT EVAPORATION LEADING TO AN INVESTIGATION OF NUCLEAR DATA) is a Monte-Carlo code dedicated to the calculation of fission observables (spectra and multiplicities of the prompt neutron and gamma particles; energies released; fission yields and more) [1]. A typical FIFRELIN calculation is performed in two steps. First, the characteristics of the two fission fragments (mass, nuclear charge, kinetic energy, excitation energy, spin, parity) are determined. Then the fragments are de-excited by prompt emission of  $n/\gamma/e^-$ . Three different pre-neutron mass yields, shown on the left-hand side of Fig. 1 are used. Yields calculated using GEF version 2021-V1.1 [2] are given by the black curve. Yields measured by Geltenbort [3], shown in the red curve, were obtained using the  $2E-2\nu$  experimental technique at the Cosi Fan Tutte mass spectrometer of the Institute Laue Langevin in Grenoble, France. Yields measured by Göök [4], green curve, using the  $2E$  technique, typically have a poorer mass resolution than that obtained with the  $2E-2\nu$  method.

The same pre-neutron Kinetic Energy distributions, measured by Göök [4], were adopted for use with all three pre-neutron emission yields.

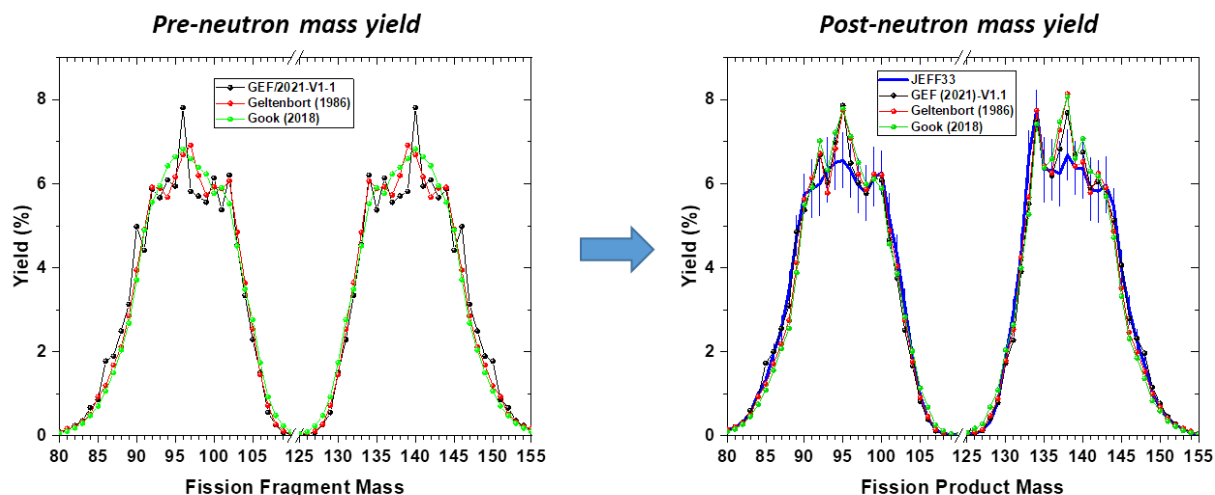


FIG. 1. Left: The pre-neutron mass yields used in three FIFRELIN calculations. Right: The three resulting post-neutron mass yields, compared with JEFF-3.3.

In these FIFRELIN calculations, the following descriptions of the spins and level densities were adopted: an energy-dependent spin cut-off, used to determine the fission fragment spin distributions and level densities based on HFB calculations and tabulated in the RIPL-3 database [5].

Using these models, the prompt gamma multiplicity as a function of the pre-neutron mass,  $\bar{M}_\gamma(A)$ , measured by Travar [6] for  $^{252}\text{Cf}(\text{sf})$  can be well reproduced by FIFRELIN (see Ref. [7] for details).

As shown on the right-hand side of Fig. 1, the post-neutron mass yields obtained by FIFRELIN are in reasonable agreement with JEFF-3.3, independent of the pre-neutron mass yields (GEF, Geltenbort or Gök). Thus, the post neutron mass yields more strongly depend on the average prompt neutron multiplicity as a function of fragment mass (sawtooth) than the pre-neutron mass yields. Nevertheless, we can also see that the structures of the post-neutron mass yields described by JEFF-3.3 are well reproduced by FIFRELIN, in particular when using the GEF pre-neutron mass yields.

#### References:

- [1] O. Litaize, O. Serot, L. Berge, Eur. Phys. J. A **51** (2015) 177.
- [2] K.-H. Schmidt, B. Jurado, C. Amouroux, and C. Schmitt, Nucl. Data Sheets **131** (2016) 107-221.
- [3] P. Geltenbort, F. Gönnerwein, and A. Oed, Radiat. Eff. **93** (1986) 57-60.
- [4] A. Gök, F.-J. Hamsch, S. Oberstedt, et al., Phys. Rev C **98** (2018) 044615.
- [5] <https://www-nds.iaea.org/RIPL-3/densities/level-densities-hfb/>
- [6] M. Travar, V. Piau, A. Gök, et al., Phys. Lett. B **817** (2021) 136293.
- [7] V. Piau, O. Litaize, A. Chebboubi, et al., Phys. Lett. B **837** (2023) 137648.

#### Q & A, Comments (C)

Q (R. Capote): Do you assume emission from fully accelerated fission fragments?

A: Yes.

C (R. Capote): Prompt neutron emission during fragment acceleration changes the shape of the PFNS.

C (A. Tudora): The use of two different  $Y(A, \text{TKE})$  data (of Straede and Al-Adili) as input to the DSE code leads to the same structure of  $Y(A_p)$ , i.e. the position of pronounced peaks and dips in the structure of the yields does not change (as shown in her presentation). Thus the same features are seen in both  $Y(A_p)$  results of FIFRELIN and DSE (i.e. using different pre-neutron fragment distributions  $Y(A, \text{TKE})$  does not change the position of pronounced peaks and dips in the  $Y(A_p)$  structure.

Q (F. Kondev): What about conversion electrons (i.e. Brevar's procedure)?

A: Up to now, the emission of conversion electrons was handled by FIFRELIN only through the

internal conversion coefficient tabulated into RIPL-3 database. Currently, a (weak) coupling with the BrIcc code (developped by T. Kibédi et al., Nucl. Instr. and Meth. A 589 (2008) 202-229) was implemented.

Q (R.Capote): Which initial (pre-neutron) fragments lead to pronounced peaks in the structure of  $Y(A_p)$ ?

A (A. Tudora): Similar to the DSE results, the pronounced peaks in  $Y(A_p)$  are due to even-Z pre-neutron fragments: the peak at  $A_p = 134$  is due to the even-odd nucleus  $^{135}\text{Te}$  while the peaks at  $A_p = 138$  and  $94$  are due to even-even pre-neutron emission fragments  $^{140}\text{Xe}$  and  $^{96}\text{Sr}$ , respectively. On the other hand, the pronounced dips in  $Y(A_p)$  are due to odd-Z pre-neutron emission fragments, highlighting the important role of the even-odd Z effect.

## 2.4 New FY evaluation methodology for JEFF-4.0 and Post-JEFF-4.0, G. Kessedjian, S.M. Cheikh, O. Serot, A. Chebboubi, D. Bernard, V. Vallet, R. Mills, L. Capponi

Fission yield evaluations represent the synthesis of experiment and theory to obtain the best estimates of the independent and cumulative fission yields. Currently, the lack of correlations between the fission yield observables induces inconsistencies in the fission yield evaluations. In the last decade, several ways to estimate the correlations of the independent fission yields satisfying the consistency with the chain yield evaluations have been proposed [1–5]. None of them a priori introduce correlations between the independent and chain yield evaluations which can arise from the reduction of experimental data.

Covariance matrices of fission yields depend on the evaluation method, according to the details of existing measurements. Their consistency is deeply entangled with the statistical agreement between each dataset, considering the covariance of the measurements. Moreover, covariances between model parameters are not the only contributions to the evaluated covariance matrix. Thus, a new evaluation process for fission yields is crucial to provide a complete and coherent evaluation. In collaboration with NNL, the LEPH Laboratory of CEA Cadarache is developing a program for future versions of the JEFF-library.

### 2.4.1 New methodology for FY evaluation

Mass yield measurements,  $Y(A)$ , are crucial for the analysis of thermal-neutron-induced fission. Indeed, the independent yields can be modeled as the product of the mass yields  $Y(A)$  and the charge and isomeric probability distributions,  $P(Z/A)$  and  $P(I/A,Z)$  respectively. This decomposition is principally due to the fact that – in reactions with direct kinematics – the nuclear charge yields are currently not separated using Frisch grid double ionization chamber for typical kinetic energy of 1 MeV/A. Thus, charged particle analysis allows reasonable mass separation but not necessarily good charge identification. Nevertheless, Gamma spectroscopy probe is a solution for nuclear charge measurements, but the limits of nuclear structure knowledge induce a parcelled description of independent fission yields. Thus, the decomposition of independent fission yields has to be consistent with the other observables at thermal neutron energy.

Correlation information comes from mass and charge conservation as well as the experimental systematic uncertainties due to the analysis procedure. The CEA is developing a statistical analysis to compare the available measurements, associating regular statistical variables to each fission yield observable. Moreover, considering the decay matrix (the  $Q$  matrix), the coupling between independent and cumulative yields need to consistently consider the chain yield data corresponding to the most precise existing data. At the end of 2022, new consistent  $^{235}\text{U}(n_{\text{th}},f)$  independent and cumulative yields were proposed and tested by the JEFF Group.

### 2.4.2 Status of the $^{235}\text{U}(n_{\text{th}},f)$ FY evaluation for JEFF-4T2: tests and validation

In this part, we presented the results of the different analysis procedures of the new fission yield evaluation methodology applied on the  $^{235}\text{U}(n_{\text{th}},f)$  reaction [6]. We describe the sorting of datasets, the selected data used and the origin of the correlation matrices of each observable. Two approaches are proposed (Fig. 1): the conservative one considering all available data but with additional uncertainty in order to validate the statistical compatibility test; the strict approach with a sorting of available data

in order to satisfy compatibility statistical test. For the first time, independent and cumulative yields are consistent in mean values, variances and covariance. Results are compared to the existing evaluations (Fig. 2). Comparison of several important cumulative yields has been discussed during the meeting. Preliminary results on the impact of the new evaluations on the reactor observables (the reactivity loss and the decay heat calculations) were presented.

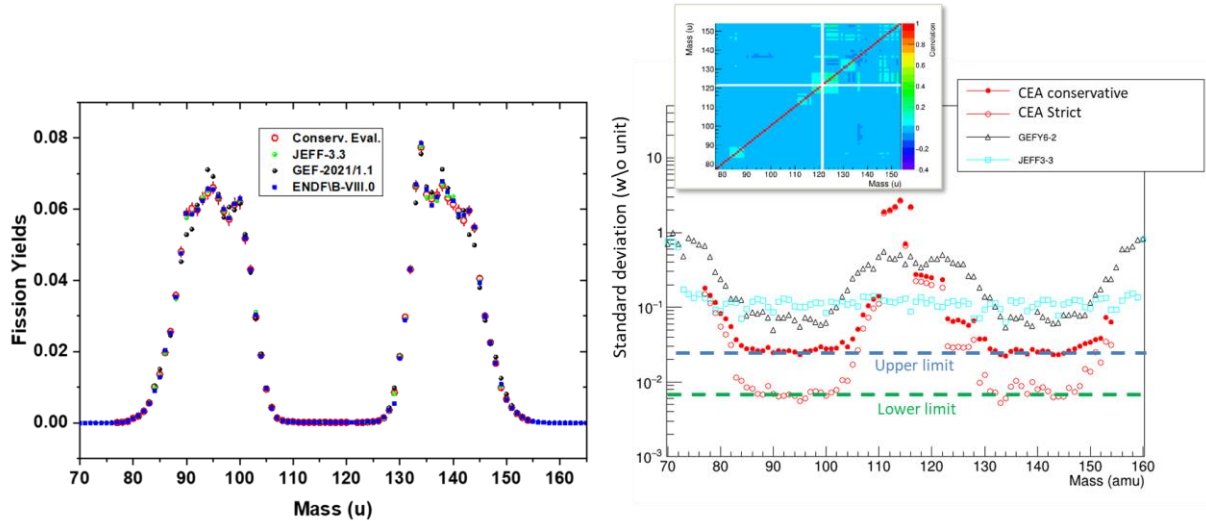


FIG. 1. Left: Mass yield evaluations and GEF models of  $^{235}\text{U}(n_{th},f)$  reaction. Right: Mass yield uncertainties according to the two proposed approaches (strict and conservative).

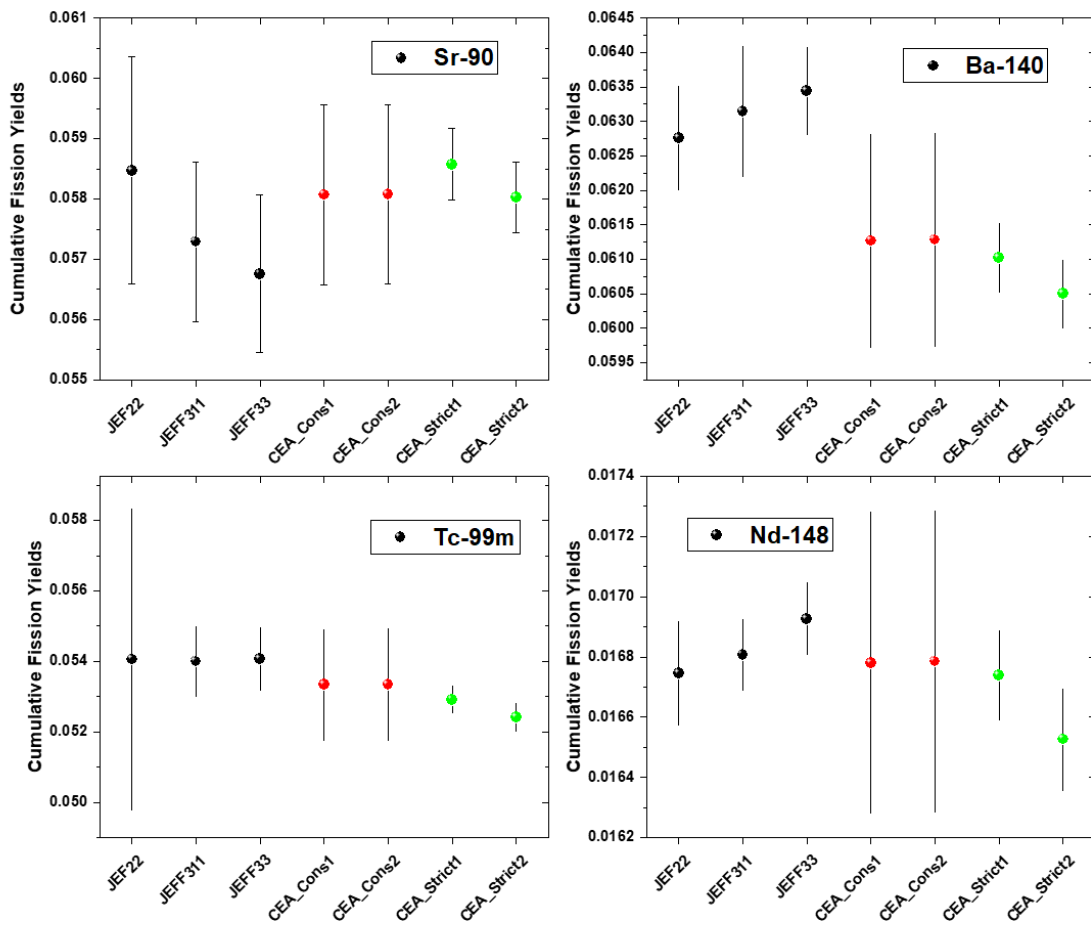


FIG. 2. Important cumulative yields in comparison to previous JEFF evaluations.

## References:

- [1] C. Devillers, The importance of fission product nuclear data in reactor design and operation, IAEA Panel, Petten, 1977, Report IAEA-213(V.1).
- [2] S.M. Cheikh, et al., Test of models for isotopic yield evaluation and their impact on the covariance analysis, jefdoc-2205.
- [3] G. Kessedjian, S.M. Cheikh, et al., Covariance analysis of  $^{235}\text{U}(\text{n}_{\text{th}},\text{f})$  independent and cumulative fission yields : propositions for JEFF4, CW 2022 Conference, EPJ Web Conf. **281** (2023) 00022.
- [4] S.M. Cheikh, G. Kessedjian et al., From fission yield measurements to evaluation: propositions of  $^{235}\text{U}(\text{n}_{\text{th}},\text{f})$  Fission Yields for JEFF-4, ND 2022 Conference, EPJ Web Conf. **284** (2023) 08002.
- [5] S.M. Cheikh, G. Kessedjian, et al., Test of models for  $^{235}\text{U}(\text{n}_{\text{th}},\text{f})$  charge distributions and their impacts on the covariance analysis, CW 2022 Conference, EPJ Web Conf. **281** (2023) 00023 .
- [6] G. Kessedjian, et al., Update of  $^{235}\text{U}(\text{n}_{\text{th}},\text{f})$  independent fission yield evaluation and news on  $^{239}\text{Pu}(\text{n}_{\text{th}},\text{f})$  IFY, jefdoc-2247.

## 2.5 New experimental data on $^{235}\text{U}(\text{n}_{\text{th}},\text{f})$ mass yields using the Lohengrin mass spectrometer (preliminary), G. Kessedjian

Today, fission yield evaluations are mainly based on experimental data because the predictive modeling capabilities for fission yields is not yet sufficiently accurate. A collaboration between the CEA, the LPSC and the ILL to measure actinide fission yields with the Lohengrin spectrometer has been in progress for several years. However, accurate measurements in the symmetric fission region as well as in the heavy region are difficult due to the significant contamination from other fragments with much higher yields and it requires the development of a new experimental setup.

This presentation first showed results of a new absolute measurement of the  $^{235}\text{U}(\text{n}_{\text{th}},\text{f})$  mass yields using an ionization chamber placed at the exit of the spectrometer. Although very well documented in the literature, these yields have uncertainties between 3% and 10% with large discrepancies among libraries, together with and a lack of correlation matrices. New experimental data obtained at the Lohengrin spectrometer was discussed, along with discussions of the measurement method and how the experimental covariance matrix was obtained. Preliminary results from the new measurement were compared to the new fission yield evaluations of the JEFF collaboration [1].

A Time of Flight (ToF) measurement has been introduced in order to improve the background rejection in the mass yield measurements [2]. In the symmetry region, the precision of the measurement is limited by backgrounds arising from charge exchange with the residual gas of the separator. In the future, we expect to analyze the data using triple coincidence measurements ( $E \times E$ )  $\times$  ToF rather than the ( $E \times E$ ) coincidence currently in use.

## References:

- [1] M. Houdouin-Quenault *et al.*, New accurate measurements of  $^{235}\text{U}(\text{n}_{\text{th}},\text{f})$  mass yields on Lohengrin spectrometer, jefdoc-2204, <https://www.oecd-nea.org/dbdata/jeff/1401-1500.html>
- [2] M. Houdouin-Quenault, C. Sage *et al.*, EPJ Web Conf. **284** (2023) 04003.

## Q & A, Comments (C)

Q: Is there an effect in other regions for nano-second isomers?

A: Yes, possibly for mass regions 137 and 100-110. The impact in the light mass region is lower than in the heavy mass region. Possibly also for two or three isomers in the mass region of 150. Also see in the mass region 140 – can do mapping to KE and unit charge. But in the 150 region, the yield is low so we have only one state per mass. For U it is possible but for Pu target, it's difficult to have the mapping. So in the new evaluations, we have to include additional uncertainty of a few percents (5-8 %). A minimum addition of 3% to the uncertainty, but 5% is not unreasonable, too, considering all effects.

## 2.6 Preliminary results of $^{252}\text{Cf}$ spontaneous fission isotopic yields via mass measurements at the FRS Ion Catcher, I. Mardor, T. Dickel

We present a new method to measure independent isotopic fission yields (IIFYs) and isomeric yield ratios (IYRs) based on direct ion counting, using a spontaneous fission (SF) source installed in the FRS Ion Catcher (FRS-IC) at GSI. Fission products (FPs) are generated by a SF source inside a cryogenic stopping cell (CSC), thermalized and stopped within it, and then extracted and transported to a multiple-reflection time-of-flight mass-spectrometer (MR-TOF-MS). Our MR-TOF-MS's relative mass accuracy ( $\sim 3 \times 10^{-8}$ ) and mass resolving power ( $\sim 1,000,000$ ) are sufficient to separate all isobars and low-lying isomers (at excitation energies as low as  $\sim 200$  keV) in the FP realm.

The first SF measurement campaign took place during the spring of 2020. A  $\sim 20$  kBq  $^{252}\text{Cf}$  source was installed in the CSC in its standard configuration, optimal for relativistic heavy ions from the GSI accelerator and the FRagment Separator (FRS). The CSC extraction time was less than  $\sim 200$  ms. The MR-TOF-MS was operated in broad-band mode, with a mass resolving power of  $\sim 320,000$  that covered  $\sim 10$  amu/e at once. IIFYs were measured for 51 FPs in the high-mass fission peak ( $56 < Z < 62$ ,  $143 < A < 161$ ), for yields as low as  $10^{-5}$ , which were extracted doubly-charged from the CSC.

We convert the counts in MR-TOF-MS mass peaks to IIFYs by considering numerous efficiency and transmission factors. The CSC stopping efficiency includes a geometrical part that is calculated analytically. It depends on the range of each FP in the relevant materials, obtained from the code ATIMA. Kinetic energies are assigned to each pair of FPs via energy and momentum conservation, assuming binary fission of  $^{252}\text{Cf}(\text{sf})$  with no prompt neutrons nor gammas. This interim approach will be replaced with a GEANT4 simulation, including the CAD model of the CSC and fission events generated by GEF. Global efficiencies and transmissions are measured with  $^{224}\text{Ra}$  doubly charged recoils from a  $^{228}\text{Th}$  recoil  $\alpha$  source, which is installed in the CSC in a location similar to the spontaneous fission source.

The FPs can undergo chemical reactions with contaminants in the CSC helium buffer gas and residual gas in the RFQ beam line and MR-TOF-MS. This leads to element-dependent efficiency factors that cannot be modelled, nor measured independently. We extract these chemical factors in a self-consistent way by considering that the chemical factors are equal for all isotopes of the same element and that the sum of IIFYs of mass chains are constrained by well-known mass yields.

Our preliminary results are mostly consistent with the ENDF and JENDL evaluations as well as previous measurements, exhibiting the expected neutron number trends for all measured elements. Nevertheless, systematic offsets are observed at the edges of our measurement region, calling for further scrutiny of our analysis procedure. This is planned with more data sets that were measured in the same region in addition to synthetic data sets produced by simulations.

We recently commissioned SF experiments with a dedicated internal part of the CSC (DC cage), where the SF source is mounted on axis and is easily replaceable. Physics measurements of SF with this setup are foreseen beginning in 2023.

The use of SF sources in the FRS-IC required extensive investment in radiation safety measures, including work on the CSC inside a special radiation safe tent, to ensure that the area is not contaminated by long-lived fission products or remnants of the SF sources. We are currently preparing radiation shielding around the CSC and special instrumentation (e.g., a glove box) that will enable experiments with a high activity  $^{252}\text{Cf}$  SF source ( $\sim 10$  MBq) and a  $^{248}\text{Cm}$  SF open source ( $\sim 30$  kBq).

### Q & A, Comments (C)

Q: Assuming that there is no prompt neutron and gamma emission from the fragments is obviously wrong.

A (I. Mardor): Yes, this is indeed a wrong assumption, made in order to simplify the stopping efficiency calculation (the distance the fission product travels inside the detector). Given all other

uncertainties, this is reasonable. In parallel, generating events with GEF and put them into GEANT4 where they have a nice model of the CSC, one can do the modeling “by the book” to see if the assumption that the error is not large is correct. However, the energy correction could be up to 20%; the question is how much this effect propagates to the error on the stopping range of the ions. The actual detector efficiency is higher than quoted because neutron and gamma emission are not taken into account.

C: The problem is that there are correlations between neutrons, gammas, and fission products, which could cause different efficiencies for different fission products. This could impact the quality of the data. Neglecting neutron and gamma emission will change both the fragment mass and the energies.

A: A good fission event generator is needed to correctly model the neutron/gamma/fission fragment correlations. Fission generation in GEANT leaves something to be desired, so they are taking output from GEF to put into GEANT. They only need to follow the fission products to calculate the range of the fission fragments. With the new experimental system, one can change the opening angle of the source and then measure the range of the fragments by changing length and pressure to ensure the range is right. At very high densities, fission fragments are all stopped in the gas, and then the simulation method is immaterial.

Q: How do you validate Monte Carlo simulations?

A: Variation of various parameters, such as opening angle of the fission products, etc. It is also possible to validate with other sources such as thorium, which have one or a few outgoing isotopes, without complicated fission events.

Q: In the future, which part of the FAIR project is the experiment under?

A: The experiment will be performed with the next generation ion catcher, at the high-energy branch of the Super-FRS. It is part of NUSTAR, the highest priority of FAIR, whose high-energy branch will be built first.

## 2.7 Progress in experiment, theory and evaluation of fission yields at CNDC, N Shu, S. Liu, Y. Chen, L. Liu

Recent progress on fission yield experiments, theory and evaluation at the China Nuclear Data Center (CNDC) are presented.

The FFIS (Fission Fragment Identification Spectrometer) for determining independent fission yields has been developed based on the  $E-\nu$  method. By directly measuring the time-of-flight (ToF) and kinetic energies of fission fragments, the post-neutron emission mass distributions of thermal neutron induced  $^{235}\text{U}$  and  $^{239}\text{Pu}$  fission were obtained with a mass resolution of  $\sim 1$  amu for the light fragment (Fig. 1). Charge identification of the fission fragments is performed with X-ray and range measurements: The fragment charge for  $39 < Z < 62$  can be resolved and the charge distributions of light fragments are promising.

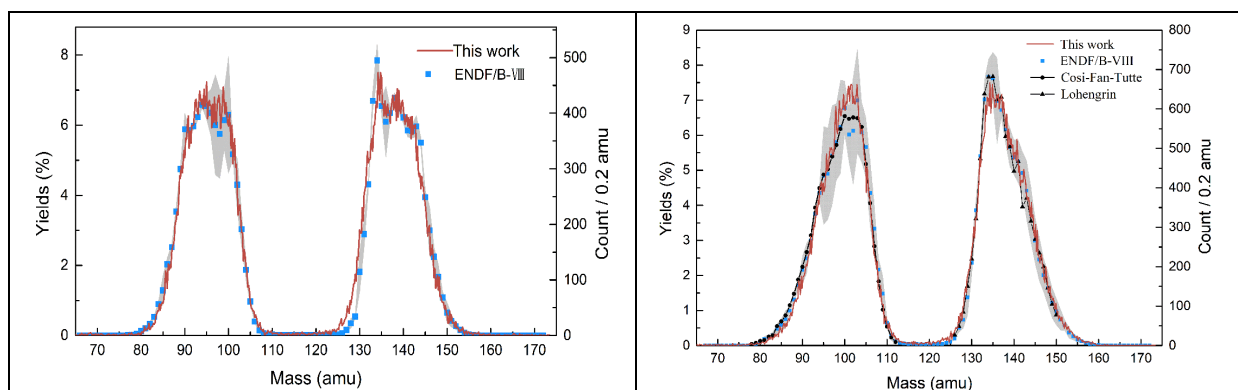


FIG. 1. The mass distributions of the  $n_{th}+^{235}\text{U}$  (left) and  $^{239}\text{Pu}$  (right) fissions



Three-dimensional Langevin approaches were applied to study nuclear fission dynamically, based on the macroscopic-microscopic model. The nuclear shape is described using a Fourier parameterization and the two-center shell model, respectively. The fission fragment mass distributions (FFMD) and the TKE distributions of some major actinides were investigated, and the results show good agreement with the experimental data (Fig. 2).

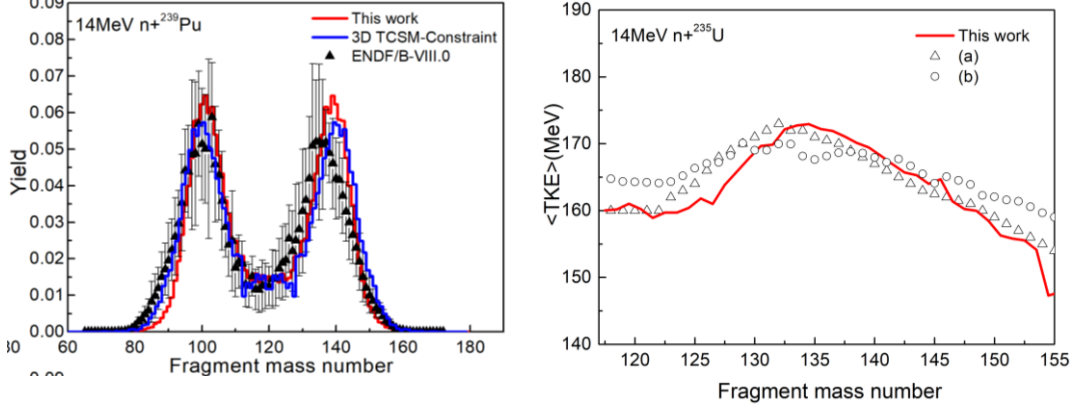


FIG. 2. The calculated FFMD for  $n+^{239}\text{Pu}$  and TKE for  $n+^{235}\text{U}$  with Fourier parameterization

Three-dimensional (the quadrupole deformation  $\beta_2$ , octupole deformations  $\beta_3$  and the number of nucleons in the neck  $q_N$ ) constrained CDFT (covariant density functional theory) calculations using the PC-PK1 functional parameter set have been performed to calculate the three-dimensional potential energy surface ( $\beta_2$ ,  $\beta_3$ ,  $q_N$ ) for fission of  $^{236}\text{U}$ , and the fission dynamic calculation based on the three-dimensional PES of  $^{236}\text{U}$  is in progress (Fig. 3).

The influence of the temperature on the fission process was investigated for neutron-induced fission of  $^{239}\text{Pu}$  using finite-temperature density functional theory (FT-DFT) with the Skyrme force. The calculated fission fragment mass distributions for  $^{239}\text{Pu}(n,f)$  based on TDGCM+GOA give a reasonable description of the increase in the symmetric fission channel with incident neutron energy.

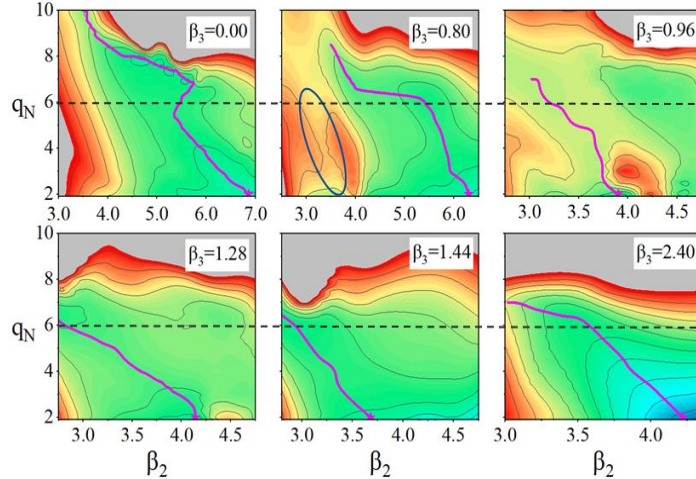


FIG. 3. Contour plots for the sections of the 3D PES of  $^{236}\text{U}$  based on CDFT

An evaluation method for fission yields was established based on the  $Z_p$  model, and the independent and cumulative yields on the same mass chain could be fitted simultaneously. Evaluation work has been done for neutron induced  $^{235}\text{U}$  and  $^{239}\text{Pu}$  fission based upon the experimental data from the EXFOR library. Fig. 4 shows the evaluation cases of  $A = 87$  and  $144$  yields from  $n_{\text{th}} + ^{235}\text{U}$  fission. For  $A = 140$ , the fitted independent and cumulative yields are close to those from ENDF/B-VIII.0 and JEFF-3.3, though there are some abnormal experimental data. However, for  $A = 87$ , the experimental data are dispersed, the results are quite different, such as the independent yields of  $^{87}\text{Se}$  and  $^{87}\text{Kr}$ , cumulative yields of  $^{87}\text{Br}$ .

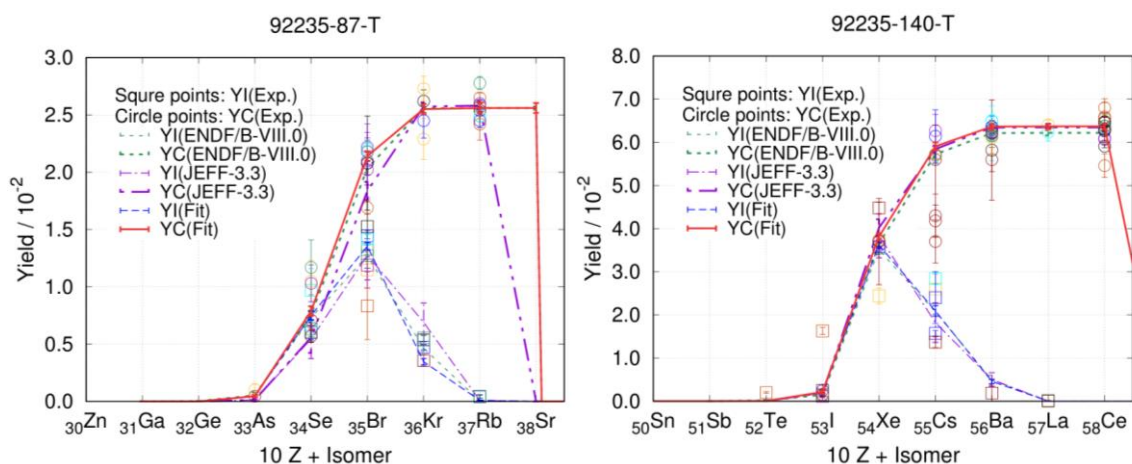


FIG. 4. Results of  $n\text{th} + {}^{235}\text{U}$  fission yield evaluation ( $A=87$  left,  $A=140$  right)

## 2.8 Fission yield compilation status, B. Prytichenko

Compilations are still missing works from authors who are alive and could provide information that is not currently included. It is a best practice to provide the data to EXFOR when they are finalized, even if the data cannot be provided within the time period of this CPR. In addition, publications don't always have all the information needed for inclusion in EXFOR (e.g., there is not enough space for tables in some publications). Experiments should try to provide data directly from the measurements, not necessarily all the fits and other analysis. Absolute measurements may not be available when ratios are measured. (There is a question about how much data should be provided e.g. should raw data be provided?). Some evaluations include data of unknown origin. Data that exist only in a thesis should be avoided because the student has likely left the field without making the final corrections.

In papers with the data given only in plots, the EXFOR compilers try to contact the authors to get the tabulated data. The compilers do not always get a positive response and then have to digitize the data. Tools for doing this relatively accurately did not exist until the late 20<sup>th</sup> century. All authors should be encouraged to share their data or publish supplementary tables. Experiments are expensive so they cannot necessarily be redone easily.

Information can be missing when the data has to be digitized so this procedure should be a last resort. No reason that recent measurements can't be put directly into EXFOR. A publication is not the end of the road.

### Q & A, Comments (C)

Q: You said you were working with ORNL and LANL to include tabulated data, are you working with anyone else?

A: We would be happy to work with other people to continue to compile missing reaction data sets. Significant information is needed to include the data in EXFOR (facility, reaction, etc.) and be useful for users. Maybe have POCs in various labs and encourage people to share their raw data.

Suggestion: Ramona and Boris organize something through the DNP.

Comment on this suggestion: Several factors show a movement in this direction. Sponsoring agencies are requiring data management plans and release of data. How this will be handled in a reasonable way and to what level of detail is a good question and is still being discussed. One approach does not fit all. In addition, Denise Neudecker (LANL) has proposed and produced uncertainty templates that experiments should use to cover all relevant uncertainties and produce covariances.

Q: You mentioned that hundreds of references still need to be included in EXFOR. Can you send the lists of references to the group?

A: Yes, these are NNDC memos already on NNDC website ("Memos").

C: A recommendation should be added to the final report to encourage experimentalists to share their data. Roberto usually includes publication information and the EXFOR number.

## 2.9 I. Influence of energy partition in fission and pre-neutron fragment distributions on independent FPYs ( $Y(Z, A_p)$ , $Y(A_p)$ ) and on kinetic energy distributions of post-neutron fragments. II. Correlation between the excitation energy of pre-neutron fragments and the kinetic energy of post-neutron fragments. Application for $^{235}\text{U}(n_{\text{th}}, f)$ , A. Tudora

The post-neutron fragment yields (independent FPYs)  $Y(Z, A_p)$ ,  $Y(A_p)$  provided by the Deterministic Sequential Emission (DSE) model describe the experimental EXFOR data very well. An investigation of the influence of the energy partition in fission and pre-neutron fragment distribution  $Y(A, \text{TKE})$  on the independent FPYs and the kinetic energy distributions of post-neutron fragments ( $\text{KE}_p$ ) is reported in Ref. [1].

We have thus used two reliable experimental  $Y(A, \text{TKE})$  data sets measured at JRC Geel by Straede *et al.* and Al-Adili *et al.*, respectively, see Ref. [1] and references therein, in this study. Two methods of TXE partition (differing as principle) are also used: our method based on modeling at scission, see Ref. [1], currently employed in the Point-by-Point (PbP) and DSE models and TXE sharing, based on the temperature ratio of complementary fragments at full acceleration  $R_T = T_L/T_H$  (employed in the CGMF and HF<sup>3</sup>D codes) by considering the fixed value,  $R_T = 1.2$ , for all fragmentations, as in the HF<sup>3</sup>D code.

This investigation has revealed that the influence of the TXE partition is visible in the  $Y(A_p)$  structure and in the structure of  $Y(N_p)$  as well: the position of pronounced peaks and dips remains the same but the positions of other, less pronounced, peaks and dips are changed. This is exemplified in Fig. 1 [1] showing  $Y(A_p)$  from DSE with the TXE partitions based on scission modeling (red) and  $R_T = 1.2$  (blue) compared to the experimental data from EXFOR (open black symbols). The pronounced peaks at  $A_p = 134$ , 138, and 94 are due to even-Z fragments ( $^{135}\text{Te}$ ,  $^{140}\text{Xe}$ , and  $^{96}\text{Sr}$  respectively) while the pronounced dips at  $A_p = 141$ , 136, 97 are due to odd-Z fragments ( $^{143}\text{Cs}$ ,  $^{137}\text{I}$ , and  $^{99}\text{Y}$  respectively), highlighting the important role of the even-odd charge effect. The energy partition does not have a strong influence on the  $\text{KE}_p$  distributions [1].

The influence of the  $Y(A, \text{TKE})$  distribution of pre-neutron fragments is observed only in the magnitudes of pronounced peaks and dips in the  $Y(A_p)$  structure (reflecting the behavior of the pre-neutron emission mass yields  $Y(A)$ ), while their positions remain unchanged. On the other hand, the kinetic energy distributions of post neutron fragments only reflect the differences between the kinetic energy distributions of fragments prior to neutron emission [1].

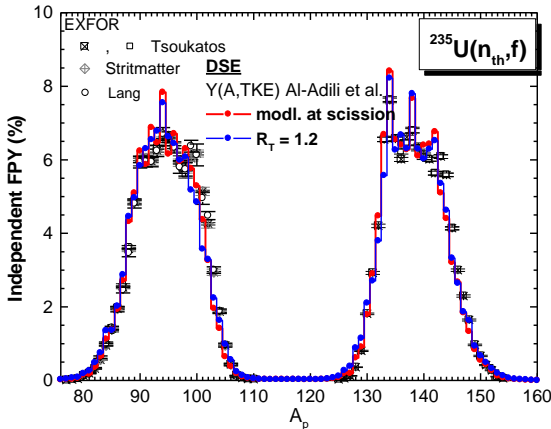


**Fig.1:**  $Y(A_p)$  results from DSE with the TXE partition based on modeling at scission (red) and  $R_T = 1.2$  (blue), together with the experimental data from EXFOR (open black symbols).

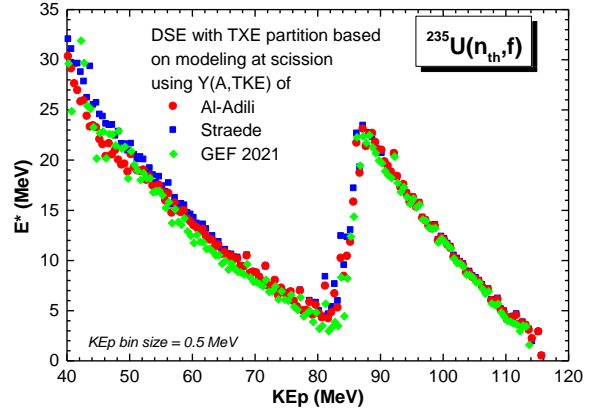


**Fig.2:**  $E^*(\text{KE}_p)$  from DSE with the TXE partition modeled at scission based on three  $Y(A, \text{TKE})$  distributions: two experimental (red and blue) and one calculated with GEF (green).

A correlation between the excitation energy of fully accelerated fragments ( $E^*$ ) and the kinetic energy of post neutron fragments ( $KE_p$ ) was observed [2]. The excitation energy as a function of  $KE_p$  exhibits a sawtooth shape, as seen in Fig. 2, consisting of two almost linear decreases which correspond to the heavy and light fragments from asymmetric fragmentations and a sudden increase linking these decreasing parts, which corresponds to both fragments from near symmetric fragmentations.  $E^*(KE_p)$  looks as a reflection in mirror of the shapes exhibited by the prompt neutron multiplicity  $\nu(A)$  and  $E^*(A)$  [2]

#### References:

- [1] A. Tudora, Eur. Phys. J. A **58** (2022) 126.  
 [2] A. Tudora, Eur. Phys. J. A **58** (2022) 258.

#### Q & A, Comments (C)

C:  $R_T = 1.2$  was proposed in PFNS studies in ~2012/-015 during the PFNS CPR; probably the physics is the same.

A: The physics is not the same at all because there are two different points of view regarding the energy partition in fission: one is based on a modeling at scission and another consists of an input parameter used for the sharing of TXE directly at the full acceleration of fragments. Both results compared to data are okay. The total average  $\langle R_T \rangle$  value obtained with the TXE partition based on modeling at scission is very close to that used as input parameter in HF<sup>3</sup>D, i.e.  $R_T = 1.2$  (which was obtained from the fit of experimental  $\nu(A)$  data). This fact can be considered as a validation “in cross” of both TXE partitions that based on modeling at scission and that using  $R_T=1.2$  as input.

#### 2.10 Report on the results of the modeling subgroup, F. Minato

Co-authors: A. Chebboubi, O. Serot, G. Kessedjan, O. Litaize, A. Tudora,, K.-H. Schmidt, S. Okumura, A. Koning, T. Kawano, O. Iwamoto.

The result of the modelling subgroup was reported during the CRP meeting. The purpose of this group is to verify results of model codes on fission yield calculations used various groups through a mutual check. The expected goal is to specify key ingredients to reproduce experimental data and improve the model codes. The contributed codes (the developers) are FIFRELIN (A. Chebboubi, O. Serot, and G. Kessedjian), PbP/DSE (A. Tudora), GEF (K.-H. Schmidt), TALYS (S. Okumura and A. Koning), BeoH (T. Kawano), and CCONE (F. Minato and O. Iwamoto).

We have carried out three tasks. The first one is to check statistical models implemented in the codes. We used <sup>139</sup>Xe at an excitation energy of 15 MeV and  $J^\pi = 5/2^+$  as a test nucleus and calculated the evaporation residues. We obtained good agreement of the production probabilities of evaporation residues. We considered that some deviations found may arose from different level densities that each code used. The second task was similar to task 1 except that now the excitation energy was assumed to be given by a Gaussian function with a mean energy of 15 MeV and a width of 3 MeV. Again, we found a good agreement among the production probabilities. By tuning the cutoff parameter of the spin distributions, differences between the models were reduced.

From tasks 1 and 2, we could confirm that the particle evaporation models give more or less similar results. The third task checked the fission yields and fission observables (prompt neutron and gamma multiplicities, prompt neutron and gamma spectra, and independent fission yields) using the same TKE and pre-neutron mass yield data  $Y(A, TKE)$  (identical to Straede et al, Nucl. Phys. A462, 85 (1987), provided by A. Tudora). We found that each model reasonably reproduced the sawtooth structure of prompt fission neutrons as a function of fragment mass. Paying attention to the  $A = 110$  region, every code using statistical models (FIFRELIN, CCONE, TALYS, and BeoH) showed similar results. However, they showed differences around  $A = 150$ . In particular, CCONE underestimated the experimental data. For prompt fission neutron spectra normalized to a Maxwellian ( $T = 1.32$  MeV), every code reasonably reproduced the experimental data at neutron energies below a few MeV, while some of them underestimated the data for an incident neutron energy of 5 MeV. Some models failed to reproduce the prompt fission gamma multiplicity data. However, PbP/DSE, FIFRELIN, and TALYS reproduced the sawtooth structure seen experimentally.

We plan to make a detailed report summarizing the activity of this subgroup in the near future.

### Q & A, Comments (C)

C (A. Tudora): The experimental  $v(A)$  data were not plotted together with the model calculations. Thus, the comparison of  $v(A)$  results with the experimental data is not as relevant because only some of the  $v(A)$  data are used. Also, the pre-neutron fragment distribution of Straede et al, is mentioned as the single distributions  $Y(A)$  and  $TKE(A)$ . In reality, the data were presented as the double differential distribution  $Y(A,TKE)$ . The full data was provided and used as input to the codes for Task 3.

C (R. Capote, T. Kawano): All models systematically do not fully reproduce the experimental PFNS data or the IAEA evaluation. The Geel PFNS data of Geel do not agree with the IAEA evaluation and there are some inconsistencies in the evaluation depending on how many data sets are used and which ones are included.

C (T. Kawano): Regarding the influence of the level density prescriptions in TALYS and BeoH, the optical model parameterization could also induce differences.

C (R. Capote): The multi-parametric  $\gamma$  strength functions may also contribute to differences. In addition, the excellent PFGS measurements must also be included in comparisons.

C (T. Kawano): The  $Y(A_p)$  results must also be compared with experimental FPY data. He noted that the default TALYS calculation ignores the spin distribution.

### 2.11 Developing the 4D-Langevin model-based fission fragment distribution database for TALYS, S. Chiba

Results of the 4-dimensional Langevin calculations for the mass and TKE distributions of fission fragments were presented. The essence of this method consists of the parameterization of nuclear shape during scission by the 2-center model. The four parameters of this model were selected as collective coordinates whose time evolution is described by the Langevin equations. The Helmholtz free energy was used as the driving potential with the single-particle energies calculated by the 2-center Woods-Saxon model. Damping of the Strutinsky shell and BCS pairing effects were carefully corrected as a function of temperature. This calculation was applied in two different ways.

First, for a precise analysis of the mass distributions of  $^{238,240,242}\text{Pu}$ , we note that the interplay of the standard I and standard II modes change the position of the heavy fragment peak, as indicated by data from Geel. The Tokyo Tech. group has reproduced this interplay by a proper combination of 2 Langevin calculations, with neck parameters of 0.25 and 0.65 fm. In this manner, the mass distributions are determined phenomenologically. We have compared the  $TKE(A)$  calculations with experimental data and found good agreement between them.

Second, we make calculations for a broad region of nuclei for astrophysical applications. Indeed, those calculations can provide mass distribution for fissioning systems with  $90 < Z < 122$  and  $221 < A < 360$ .  $TKE(A)$  data will be analysed and supplemented.

In conclusion, the Tokyo Tech. group can deliver mass and TKE distributions of fission fragments as a function of the fragment mass over a broad range of nuclei. Results will be tabulated in the near future and will be used in TALYS for decay calculation of fission fragments to yield independent as well as cumulative fission product yields.

### Q & A, Comments (C)

Q (R. Capote): What about shell corrections and, for  $\sigma(T) = \text{constant}$ , up to which T value? The answer of S. Chiba is given by showing the slide with a figure of  $\sigma(T)$ . R. Capote comments about the standard fission modes S1, S2 according to the terminology of Brosa and the names of fission modes used in this presentation.

Q (O. Serot): How does  $\sigma(TKE)$  behave for  $^{294}\text{Og}$ ? Experimentalists have seen very asymmetric peaks in the Lohengrin measurements.

A: Chiba showed a slide demonstrating the behavior of the total average masses of the heavy and light fragments:  $\langle A_H \rangle$  remains almost constant while  $\langle A_L \rangle$  increases with increasing mass of the fissioning nucleus.

Q (R. Capote): Have the authors compared the calculated  $TKE(A)$  with the experimental data for fission of U and Pu isotopes?

A: Such comparisons were presented by Chiba's students during the ND2022 conference. He also presented a slide with  $\langle TKE \rangle$  as a function of  $Z^2/A^{1/3}$  showing the contribution of the super-short fission mode for Fm, Md etc.

Q (R. Vogt): Is neutron evaporation included?

A: It was not considered. Chiba again showed a slide of the entire fission process (pre-scission, scission, prompt emission, and delayed emission) saying that GEF, TALYS and CCONE need something at scission point such as scission neutrons between  $10^{-20} - 10^{-18}$  s.

Q (S. Hilaire): Do you get four peaks in  $Y(A)$  for superheavy nuclei? In a specific region?

A: The peak in the center, near symmetry, can be divided into 2 peaks in the case of very heavy nuclei with  $Z = 122$  (near symmetry,  $A \sim 150$ ). He explains this behaviour by showing  $TKE(A)$  with contributions from the super-long and super-short fission modes. In the region of Fm fission one can say there are 2 peaks for some Fm isotopes but a single peak for others which can be explained by the influence of shell corrections.

## 2.12 Use of TALYS to calculate fission yields and neutron and gamma emission, A. Koning

Co-authors: K. Fujio, A. Al-Adili, S. Okumura.

The TALYS nuclear model code contains various new features for the prediction of fission yields and associated neutron observables. A deterministic technique for fission fragment decay is implemented allowing the calculation of prompt fission observable characteristics for a wide range of fissioning systems. The method is basically built around the calculation of de-excitation energy by treating the fission fragment as a compound nucleus.

A comparison of independent FPY of  $^{235}\text{U}(n_{th},f)$  with the results of GEF, TALYS and TALYS(HF<sup>3</sup>D) has been carried out, showing that the evaluation values of independent FPY can be reasonably reproduced after fine-tuning the TALYS input parameters so that the results of HF<sup>3</sup>D/BeoH (LANL, T. Kawano) were best reproduced.

The final results are that the PFNS result shows a softer spectrum compared to experimental data, and the PFGS result at low prompt  $\gamma$ -ray energies (below 1 MeV) is strongly dependent on the number of energy bins, the same situation holds for the case of prompt  $\gamma$ -ray multiplicity.

The results of  $\nu(A)$ ,  $M_\gamma(A)$ ,  $\langle \nu_n \rangle$ ,  $\langle \nu_\gamma \rangle$  are presented ( $\langle \nu_n \rangle$  of TALYS is 2.31, of ENDF is 2.414).

Regarding the behaviour of the total average prompt neutron multiplicity  $\langle \nu_n \rangle$  as a function of incident neutron energy  $E_n$ : differences exist between the  $\langle \nu \rangle(E_n)$  results of TALYS(GEF) and TALYS(HF<sup>3</sup>D).

The  $\beta$ -decay calculations run outside of TALYS. As for average neutron and gamma multiplicities,  $\langle \nu_n \rangle$  as a function of mass of the target nucleus (at  $E_n = 1$  MeV) shows that more neutron rich nucleus more neutron emission occurs (comparison GEF, GEF+TALYS), while  $\langle \nu_\gamma \rangle$  as a function of mass of the target nucleus (at 1 MeV) shows large differences for many actinides.

Finally, GEF(FF)+TALYS(HF decay) shows 1) relative good results for  $^{235}\text{U}(n_{th},f)$  and 2) global results for 250 actinides at 1 MeV.

### Q & A, Comments (C)

Q (J.-F.Lemaitre): What inputs are tuned by the comparison between TALYS and HF<sup>3</sup>D/BeoH?

A: We look at the spin distribution, microscopic distributions, isomeric ratios and more. There are 2 spin distributions, 3 level density models etc.

Q (J.-F. Lemaitre): Regarding the slide with  $\langle \nu_\gamma \rangle$  as a function of mass of the target nucleus at 1 MeV, why are there large differences between  $\langle \nu_\gamma \rangle$  at different mass numbers?

A: We don't know why!

Q (R. Capote): In the case of PFGS at low  $E_\gamma$  have you considered only a continuum spectrum of levels and the problem of level density prescription?

A: No, the entire gamma-ray cascade is taken into account.

### 2.13 Microscopic determination of fission fragment distributions: current status, S. Hilaire, J.F. Lemaitre

Co-authors: D. Regnier, N. Dubray, S. Goriely, R. Lasseri

So far, our plans with respect to fission yield studies have included two approaches based on the Gogny DIM effective nucleon-nucleon interaction, which has proven able to reproduce nuclear masses with reasonable accuracy [1]. More precisely, we plan to compute fission yields using either the microscopic time dependent generator coordinate method (TDGCM), following previous work [2, 3], or a less fundamental approach based on the SPY model [4, 5].

The TDGCM relies on a purely quantum mechanical approach which is performed in two steps. The first step computes the potential energy surfaces of the nucleus that is going to fission. The second step deduces the fission yields from the evolution of the nuclear wave function in the potential energy surface (PES) landscape using the FELIX code [6, 7]. The computational cost of this approach mainly stems from the need to map out the PES with a sufficiently fine grid. So far, the elongation and asymmetry are the main variables considered and while the results qualitatively agree with experimental data, they do not reach the accuracy required for evaluation purposes. Recent efforts have been devoted to allow a robust computation of the PES, which are now rather well under control, so that a systematic calculation of PESs will soon be available. FELIX can then hopefully be used to produce fission yields for all even-even nuclei of interest.

However, the analysis of the PES shows discontinuities that are believed to be responsible for discrepancies attributed to a too low number of collective variables considered in the calculation. Two solutions are possible. a) Increasing the number of collective variables, which means a significant increase in computing time and an arbitrary choice of the added collective variable without any guarantee that it will be appropriate. b) Attempting to use a machine learning approach to deduce, from the continuous part of the PES, new collective variables which will generate a new fission path free from discontinuities.

This activity is ongoing and shows promising results but will not be practically applicable before the end of the CRP.

The other approach is based on the SPY model which has the advantage of providing fission yields at a very low computational cost and also allows fine tuning of the raw results with free parameters to fit the experimental data. The SPY model is a statistical scission point model based on fully microscopic nuclear ingredients describing the fragment properties at the scission point [4, 5]. Thermal equilibrium at scission is assumed so that a statistical microcanonical treatment can be used to calculate the fission fragments' properties. The definition of the scission point is based on the proton density in the scission neck. Additionally, a corrective term is added in order to better reproduce the fission fragment yields. A smoothing procedure is used to reduced fluctuations in the raw fragment energies and yields.

Thanks to the corrective term and the smoothing procedure, an evaluation of the fission yields of neutron-induced fission of  $^{235}\text{U}$  and  $^{239}\text{Pu}$  and spontaneous fission of  $^{252}\text{Cf}$  was performed independent of the TKE distribution. Experimental data are fairly well reproduced. Large scale calculations from  $Z = 70$  to  $Z = 124$  were also performed, with excitation energies ranging from 0 to 20 MeV in steps of 2 MeV. This database was included in TALYS 1.96 and 2.0 [8].

Post-neutron emission fission yields have also been computed with TALYS using Okumura's pre-neutron emission yields [9]. Experimental data are fairly well reproduced. Additional post-neutron emission observables were also computed: PFNS, PFNM, PFGS, PFGM, and isomeric ratios. They were compared with experimental data when available. The impact of the level density models and the spin cutoff parameter have also been studied.

## References:

- [1] S. Goriely, S. Hilaire, M. Girod, S. Peru, Phys. Rev. Lett. **102** (2009) 242501.
- [2] D. Regnier, N. Dubray, N. Schunck, M. Verrière, Phys. Rev. C **93** (2016) 054611.
- [3] D. Regnier, N. Dubray, N. Schunck, Phys. Rev. C **99** (2019) 024611.
- [4] J.-F. Lemaître, S. Goriely, S. Hilaire, J.-L. Sida, Phys. Rev. C **99** (2019) 034612.
- [5] J.-F. Lemaître, S. Goriely, A. Bauswein, H.-T. Janka, Phys. Rev. C **103** (2021) 025806.
- [6] D. Regnier, M. Verriere, N. Dubray, N. Schunck, Comp. Phys. Comm. **200** (2016) 350.
- [7] D. Regnier, N. Dubray, M. Verriere, N. Schunck, Comp. Phys. Comm. **225** (2018) 180.
- [8] A. Koning, S. Hilaire, S. Goriely, Eur. Phys. J. A **59** (2023) 131.
- [9] S. Okumura, T. Kawano, P. Jaffke, P. Talou, S. Chiba, J. Nucl. Sci. Technology **55**(9) (2018) 1009–1023.

## Q & A, Comments (C)

Q (R. Capote): Do you consider an enhancement factor for level densities?

A: No, only pure intrinsic states are taken into account.

Q (O. Serot): What is the origin of the peaks?

A: These may be due to strong even-odd effects but this was not investigated in detail.

Comment (R. Capote): Since the sensitivity of neutron observables such as  $v(A)$ ,  $\langle \varepsilon \rangle(A)$  to the level densities can be large, it would be interesting to see this effect on the fission fragments.

C (T. Kawano): The level densities should affect the spin distributions, after neutron evaporation.

J.-F. Lemaitre comments that he can provide SPY results in an internal report.

R. Capote replies that tables are needed for this CRP so they should produce tables using SPY.

Q (O. Serot): Are you able to determine the isotopic yields considering your proton density?

A: This is a good suggestion, as well as to be able to produce systematic calculations.

C (R. Capote): Regarding low and high pairing along the isotopic chain, global calculations with very low pairing lead to no solutions.

A: The discontinuities arising due to the distance between neighboring points in the potential rather come from the fact that the calculation are performed in a reduced space (2 dimensions)

## 2.14 Fragment spin properties from FREYA, R. Vogt, J. Randrup

*Work performed under the auspices of the U.S. Department of Energy by Lawrence Livermore National Laboratory under Contract DE-AC52-07NA27344.*

In the last two years FREYA has been updated to study fission fragment angular momentum generation. We have also introduced integer and half integer spins, not specified in FREYA previously, and required to specify fragments more precisely. With these changes, FREYA still conserves energy as well as linear and angular momentum throughout the fission event. It is now possible to use FREYA to study a number of correlated quantities related to fragment spin, some of which can be directly measured, see Refs [1–4]. The spin-spin correlation, see Ref. [4], was a major point of discussion at the Fission Fragment Angular Momentum workshop in Seattle in June 2022 [5].

Angular momentum in FREYA is based on the nucleon exchange transport model, developed for damped nuclear reactions, discussed in detail in a number of papers and summarized briefly in Ref. [2]. In this model, multiple nucleon transfers between proto-fragments produce a dissipative force that changes the fragment linear and angular momenta. These exchanges result in rotational fluctuations that are perpendicular or parallel to the fission axis. The two wriggling (mutually parallel spins, perpendicular to fission axis) and two bending (mutually anti-parallel spins, perpendicular to fission axis) modes have been assumed to be fully agitated in FREYA heretofore [6]. The tilting and twisting modes, parallel to the fission axis and mutually parallel or mutually anti-parallel respectively, were ignored.



A comparison of the relaxation times of the modes, based on their mobility coefficients, show that the wriggling mode, the fastest, should be fully agitated within the fission time while the bending mode is likely to be mostly agitated and the twisting mode at least partially agitated [3]. The tilting mode is not directly agitated because the dot product of the orbital angular momentum with the separation between the fragment centers at scission,  $R = R_L + R_H + d$ , is zero. FREYA has been used to explore different rotational scenarios based on a mode temperature determined by the degree of twisting included,  $T_m = c_m T_{sc}$  where  $c_m = \{c_{\text{wrig}}, c_{\text{bend}}, c_{\text{twist}}\}$ . The default in FREYA is  $c_m = \{1, 1, 0\}$ . The mode amplitudes are sampled from  $P_m(s_m) \sim \exp(-s_m^2/2I_m T_m)$  where  $I_m$  is the moment of inertia of the mode. The spins of the light and heavy fragments are then  $S_L = (I_L/I_+)S_{\text{wrig}} + S_{\text{bend}} + S_{\text{twist}}$  and  $S_H = (I_H/I_+)S_{\text{wrig}} - S_{\text{bend}} - S_{\text{twist}}$ . The fluctuations in the fragment spins are compensated for by corresponding changes in orbital angular momentum, conserving total angular momentum.

The fluctuations in the rotational modes dominate the angular momentum, leading to a very weak spin-spin correlation between the fragments, even though each nucleon transfer is highly correlated. The relative moment of inertia is large compared to those of the two fragments, further reducing the initial correlations [1, 2]. In Ref. [3], two potential observables were discussed: the orientation of the spins with respect to the fragment motion, via E2 gamma transitions between even-even nuclei as a function of  $\cos(\theta_{\gamma f})$ , the relative orientation of the fragment spins. In the first case, if the spin is parallel to the direction fragment motion, an oblate distribution will result whereas, if the spin is perpendicular to the direction of motion, the distribution will be prolate. The wriggling and bending modes should primarily lead to a prolate distribution while the twisting mode will result in a more prolate distribution, as indeed observed in the FREYA calculations. As the degree of twisting is increased, the gamma yield at zero degrees relative to 90 degrees will decrease, potentially setting limits on the degree of twisting [3]. In the second case, if one could measure the opening angle distribution,  $\theta_{12}$ , between two E2 gammas with identified helicities originating from partner fragments, one could determine the correlation between spin directions. If both gammas have positive helicities, they will emerge in the upper hemisphere of the fragment plane, while those with negative helicities will emerge in the lower hemisphere. When the wriggling mode is agitated, the gammas emerge in the same hemisphere and opening angle between the two spins is small whereas, with the bending mode excited, the gammas will emerge in opposite hemispheres, with a large opening angle between them. An effect similar to bending is seen for twisting, when the photons are oppositely directed but emerge in the plane of the fragments. In the default FREYA scenario, when wriggling and bending are both fully agitated, the distribution is independent of  $\theta_{12}$ .

Finally, there have been contrasting results for the spin-spin opening angle distribution from various models. Because FREYA assumes that the spins are generally perpendicular to the fragment plane, the correlation is small, on the order of a few percent and also assumes that the fragments are relatively far apart at scission, with a 4 fm fragment separation. On the other hand, the AMD [7] and TDDFT [8] approaches do not make any assumptions about the spin direction, allowing it to be fully three dimensional. Similar to FREYA, the AMD calculation, seems to agree with well-separated fragments, resulting in an opening angle distribution peaking near 90°. On the other hand, the TDDFT calculation is peaked near 120°, equivalent to fragment overlap, a seemingly unlikely scission scenario.

#### References:

- [1] R. Vogt, J. Randrup, Phys. Rev. C **103** (2021) 014610, arXiv:2012.04155 [nucl-th].
- [2] J. Randrup, R. Vogt, Phys. Rev. Lett. **127** (2021) 062502, arXiv:2103.14778 [nucl-th].
- [3] J. Randrup, T. Døssing, R. Vogt, Phys. Rev. C **106** (2022) 014609.
- [4] J. Randrup, Phys. Rev. C **106** (2022) L051601, arXiv:2208.14941 [nucl-th].
- [5] Workshop on fission fragment angular momentum, <https://indico.in2p3.fr/event/26459> (2022).
- [6] J. Randrup, R. Vogt, Phys. Rev. C **89** (2014) 044601.
- [7] J. Chen, C. Ishizuka, A. Ono, S. Chiba, “Microscopic simulation of symmetric boost fission with antisymmetrized molecular dynamics,” <https://indico.frib.msu.edu/event/52/contributions/600/>.
- [8] A. Bulgac, I. Abdurrahman, K. Godbey, I. Stetcu, Phys. Rev. Lett. **128** (2022) 022501, arXiv:2108.03763 [nucl-th].

### Q & A, Comments (C)

Q: How do different scenarios impact the photon emission?

A: We need twisting mode focused measurements.

Q: Opening angle for the AMD case?

A: The opening angle is consistent with a standard scission configuration.

Q: Energy dependence?

A: The energy dependence is not strong.

## 2.15 Change in reactivity in a PWR pin-cell depletion benchmark using recent FY evaluations, O. Cabellos

This presentation summarizes the work presented in the “*JEFF Depletion meeting, February 10, 2021*” and in the “*JEFF Nuclear Data Week, November 25, 2021 (JEF/DOC-2111)*”. The objective is to predict the change in reactivity in a typical PWR pin-cell up to a high-burnup of 60 GWD/MTU. The specifications of the pin-cell are given in Table 1.

TABLE 1. PIN-CELL BENCHMARK FOR BURNUP CALCULATIONS

	Fuel	Cladding	Moderator
Temperature	873.0 K	608.52 K	583.0 K
Material	UO <sub>2</sub> (3.1% U-235 enrichment)	Zirconium	750 ppm Boron
Size (in cold conditions)	Outer-radius: 0.409575 cm	Outer-radius: 0.474980 cm	Pitch pin-cell: 1.259840 cm
POWERC - constant 36.22 MW/MTU			

Calculations are performed with the deterministic code WIMSD5b, using the WIMSD-69g library processed with the NJOY code:

- JEFF-3.3 and ENDF/B-VIII.0 were processed in-house using WLUP procedures with NJOY2016;
- JEFF-3.1 and ENDF/B-VII.1 are from the IAEA/WLUP Project ([www-nds.iaea.org/wimsd/](http://www-nds.iaea.org/wimsd/)).

In Table 2, a comparison of reactivity with the reference library ENDF/B-VII.1 shows that both ENDF/B-VIII.0 and JEFF-3.3 significantly underestimate the reactivity at high burnup. However, this reactivity underestimation is reduced if we use the isotopic composition predicted with ENDF/B-VII.1. So, we may conclude that the transmutation buildup is playing an important role in reactivity burnup.

TABLE 2. REACTIVITY CHANGES (in pcm) IN THE PIN-CELL BENCHMARK FOR DIFFERENT BURNUP STEPS

	ENDF/B-VIII.0 - ENDF/B-VII.1		JEFF-3.3 - ENDF/B-VII.1	
	Isotopic composition with ENDF/B-VIII.0	Isotopic composition with ENDF/B-VII.1	Isotopic composition with JEFF-3.3	Isotopic composition with ENDF/B-VII.1
BOC No Xenon	-70	-70	+235	+235
BOC Xenon Eq.	-55	-2	+380	+325
60 GWD/MTU	-550	-65	-1500	-275

**Note:** BOC = Beginning of Cycle

In order to investigate the main contributors to these differences in reactivity, simulations employing different nuclear data libraries are performed. Figure 1 shows the main contributors to  $\Delta k_{\text{eff}}$  for the JEFF-3.3 and ENDF/B-VII.1 comparisons. In this case, <sup>239</sup>Pu, <sup>238</sup>U, “Fission Yields + Decay Data and <sup>235</sup>U are the main contributors. At 60 GWd/MTU, the FY+DD contribution is around -500 pcm.

However, the effect of “FY+DD” is not seen in ENDF/B-VIII.0 because the FYs were taken from ENDF/B-VII.1.

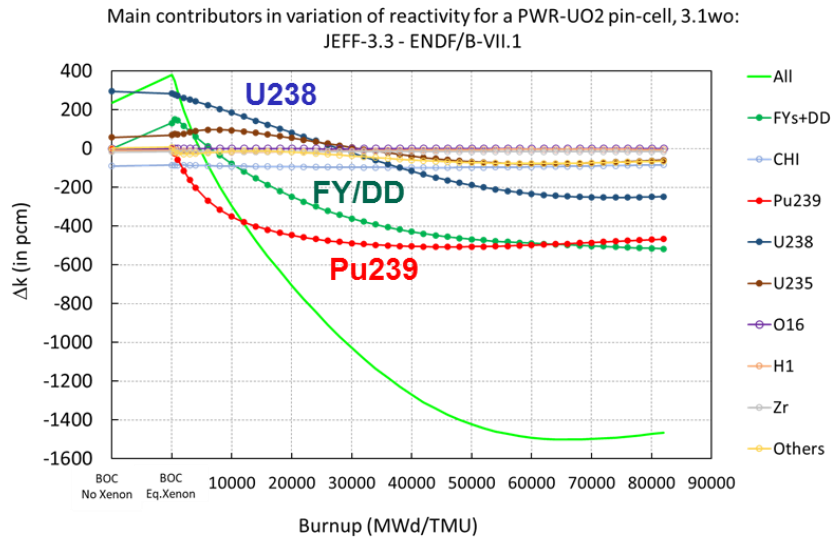


FIG. 1. Reactivity modification between J33 – E71: Main contributors

Additionally, this work includes an analysis of the impact of FY+DD in the isotopic inventory of some fission products important for reactivity:  $^{135}\text{I}$ ,  $^{135}\text{Xe}$ ,  $^{103}\text{Rh}$ ,  $^{143}\text{Nd}$ ,  $^{145}\text{Nd}$ ,  $^{147}\text{Sm}$ ,  $^{149}\text{Sm}$ ,  $^{150}\text{Sm}$ ,  $^{153}\text{Eu}$ ,  $^{155}\text{Gd}$ , and  $^{152}\text{Sm}$ , among others. An example of the impact of FYs can be seen in Fig. 2. The Figure shows differences in the  $^{147}\text{Sm}$  concentration between a given nuclear data library and ENDF/B-VII.1 as a function of the burnup. Substituting the JEFF-3.3 FYs by those of ENDF/BVII.1 will significantly modify the  $^{147}\text{Sm}$  concentration. The FY from  $^{235}\text{U}$  for  $^{147}\text{Sm}$  in ENDF/B-VII.1 is 0.0085794 while in JEFF-3.3 it is 0.010552. Such FY differences may explain the differences observed in Fig. 2.

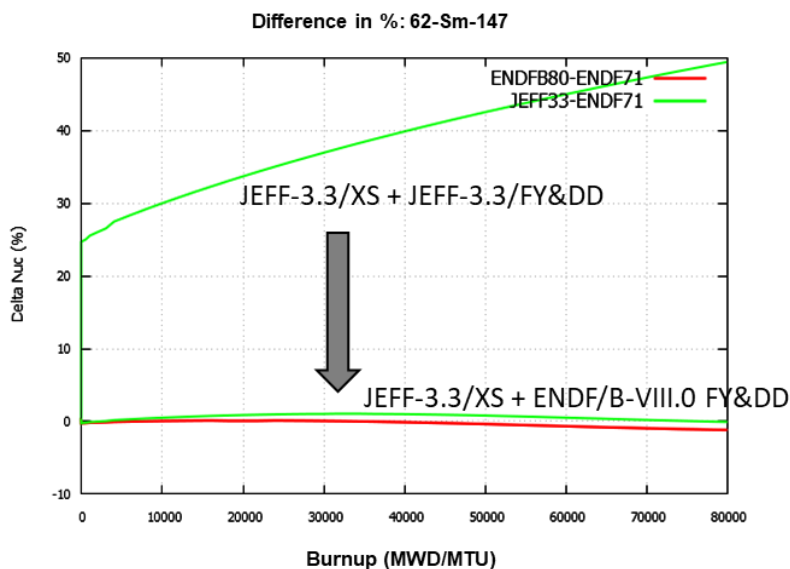


FIG. 2.  $^{147}\text{Sm}$  modification as a function of FY+DD

In conclusion, FYs nuclear data libraries may play an important role in explaining the reactivity burnup issue in the JEFF-3.3 evaluation.

### Q & A, Comments (C)

Q (Dimitriou): Are the FPYs independent or cumulative?

A: They are independent.

Follow up: It was noted that the effect he observed could also be an effect of the decay data. They should be changed in the same package, so the simulation is not just a test of the FYs alone but also of decay data. He would like to understand which isotopes contribute most to changes in reactivity. For example, changing  $^{105}\text{Rh}$  for JEFF3.3 and ENDF/B-VII.1 changes  $k_{\text{eff}}$  by 20-40 pcm. This suggests that there should be a joint evaluation for depletion of  $^{235,238}\text{U}$  and  $^{239}\text{Pu}$  fission yields and decay data because depletion affects  $k_{\text{eff}}$  differently.

Q (R. Mills): Did he change full decay data and fission yields together?

A: Yes.

Q: (P. Dimitriou): Do differences in decay data change things a lot?

A: No.

C (R. Capote): This would not be useful to define FY data but could be an interesting test of new yields.

### 2.16 Progress on UKFY3.7 development, R. Mills

There has been steady progress to release the experimental FY data used in UKFY libraries. The current experimental database contains 15836 records now, and includes measurements of cumulative, independent, and fractional yields, including ratio of ratio measurements. The original version was developed in 1962 by Cunningham, it was updated towards the JEFF-3.3 release by R. Mills in 2017.

The experimental database is in plain text, easy to process, in a fixed FORTRAN format. The processing method includes:

- 1) First, absolute measurements are processed to produce an initial estimate, then used to convert the ratio measurements to obtain a consistent set. The iteration converges relatively quickly over very few iterations.
- 2) When data disagree with the average, their uncertainties are increased - normalized residuals.

The experimental database was already released to CEA collaborators, 15899 entries will be released to NEA/IAEA in mid-2023. New US data are still not incorporated.

Are the new evaluation data for  $^{239}\text{Pu}$  FY significantly different?

$^{153}\text{Sm}$  FY from  $^{239}\text{Pu}$  thermal fission for criticality safety inconsistent, ENDF 0.36, JEFF31 0.38, and JEFF33 0.59: new measurements approved at ILL Grenoble.

A future plan includes 1) the data release to NEA/IAEA; 2) update, review new EXFOR, SFY, NFY references, energy-dependent data and, 3) continue traditional evaluations needed for JEFF using the updated database.

### Q & A, Comments (C)

Q: Does uncertainty renormalization happen at each iteration?

A: Yes

Q: Does the traditional evaluation include 3 energy groups? What about "fast"?

A: Yes

Q: How do you use the ratio data (R-value)?

A: For validating results.

Q: Can we have the average experimental data?

A: Yes, once the database is released.

C: IAEA can plot Mills' data too if provided.

## 2.17 Evaluation of fission fragment yields and parameter optimization in CCONE code system, F. Minato

We reported a test evaluation of fission yields from thermal neutron-induced fission of  $^{235}\text{U}$  using the CCONE code [1]. We studied a method of optimizing the parameters related to the fission yields. In particular, we paid attention to the parameters related to Wahl's  $Z_p$  charge distribution [2] which assumes a Gaussian distribution for atomic number. Since there are nearly 107 parameters, they were first separated into three parts for the light, heavy, and symmetric fragment regions. For the mass and TKE distributions, we used the parameters given in A. Lovell et al. [3]

To optimize the parameters, two approaches were adopted. One was the generalized least square (GLS) and another was a Bayesian optimization with a Gaussian process (BO+GP). We defined an objective function to be minimized with respect to experimental data. The GLS required 146 iterations of the CCONE calculations to obtain good convergence. On the other hand, the BO+GP method could not find a converged result successfully, even after several hundred calculations. Therefore, the GLS method seems most promising for finding the optimized parameters for the charge distributions.

However, the GLS procedure has a shortcoming. It is frequently stuck in a local minimum of the objective function, depending on the initial parameter set. In this respect, the BO+GP, which seeks parameters globally beyond local minima, is still considered to be a powerful tool. To make the best use of two approaches, we first used the BO+GP to find a plausible global parameter set. At some point, the BO+GP calculation was stopped, and the parameter set giving the lowest objective function was stored. Then, we initiated GLS using the parameter set optimized by the BO+GP procedure as the initial parameters. By combining the two approaches, here called BO+GP+GLS, we could reduce the number of CCONE calculations. For example, in the case of the three different  $Z_p$  parameter regions, only 64 CCONE calculations were needed, less than half required with GLS alone. After extending the number of parameters to 10, it was found that 250 CCONE calculations were needed for BO+GP+GLS while 924 were needed for GLS alone. After parameter optimization, we also found that the experimental independent yield data, as well as data on neutron multiplicities, and decay heats were successfully reproduced.

We are now extending this approach to increase the number of adjustable parameters and experimental data sets. We expect that better results will be obtained with this method.

### References:

- [1] O. Iwamoto, N. Iwamoto, S. Kunieda, et al., Nucl. Data Sheets **131** (2016) 259.
- [2] A.C Wahl, Report LA-13928, Los Alamos National Laboratory, Los Alamos, NM (2002).
- [3] A.E. Lovell, T. Kawano, S. Okumura, et al., Phys. Rev. C **103** (2021) 014615.

### Q & A, Comments (C)

Q: Did you use existing decay data?

A: Yes, JENDL decay data.

Q: Was only the thermal point addressed?

A: CCONE can calculate energy-dependent FPYs, but some energy-dependent parameters are still under consideration.

C: The charge distribution as a function of  $A$  may be energy dependent.

A: Shell correction damping will be incorporated in the model.

C: England and Rider compiles post-neutron-emission yields, the pre-neutron emission yields should be symmetric.

A: Result is pre-neutron, no constraint on the symmetry, we need it.

## 2.18 The ENDF re-evaluation of FPYs, A. Lovell

New work is being undertaken at Los Alamos National Laboratory to re-evaluate fission product yields for major actinides. The method combines new experimental measurements, modeling, and already compiled experimental data. There have been many new measurements recently for cumulative fission product yields, particularly those with short half-lives. Brookhaven National Laboratory is compiling all historic data and updating any data where the structure information that went into the experimental analysis has since been improved. A new model, BeoH, developed at Los Alamos National Laboratory is being used to perform calculations from thermal to 20 MeV incident neutron energies. BeoH is a deterministic, Hauser-Feshbach fission fragment decay code [1, 2] that takes fission fragment initial conditions as inputs and models the prompt and delayed decays of the fission fragments. In this way, the independent and cumulative fission product yields are calculated consistently with other fission observables, such as neutron and gamma-ray multiplicities and energy spectra.

The evaluation process combines experimental data and model calculations through a Kalman filter, leading to updated parameters that can be introduced back into the model. Covariance matrices between various fission product yields or incident energies are also consistently calculated, taking into account parametric uncertainties and experimental uncertainties. The optimization includes cumulative fission product yields, along with the average prompt and delayed neutron multiplicities.

A first-pass optimization for cumulative fission product yields for  $^{235}\text{U}$ ,  $^{238}\text{U}$ , and  $^{239}\text{Pu}$  were presented for the full range of incident neutron energies available in the model (thermal to 20 MeV). Fine tuning of the input parameters, especially for isotopes that are more well known, still needs to be performed, as all results are preliminary at this time.

Results of the evaluated fission product yields for  $^{235}\text{U}$ , from thermal to 20 MeV, were shown. The impact of multi-chance fission included in the model is clearly seen. There are slope changes in the energy-dependent fission product yields. A comparison to ENDF/B-VIII.0 is made for thermal, fast, and 14 MeV, where the previous evaluation has been performed. The overall agreement is reasonable, but more tuning has to be performed to better reproduce well-known experimental data. Covariances between fission product yields at discrete energies were shown, which are currently not included in the ENDF/B-VIII.0 library. Similar comparisons were shown for  $^{238}\text{U}$  and  $^{239}\text{Pu}$ .

Validations of select fission product yields are being performed through the calculation of R-values, by collaborator G. Rusev of Los Alamos. The neutron flux through various critical assemblies was calculated as a function of the distance from the center of the assembly. The flux was folded with the R-values, calculated from the preliminary BeoH calculations. These new results agree, within uncertainties, with historic data [3].

The next steps are to perform addition model adjustment to account for the stiffness in the model, to ensure better agreement with well-known experimental fission product yields. Additionally, a format for the full fission product yield covariances (beyond the standard deviations) is being developed. Additional studies into the fission product yield uncertainties are ongoing, including ensuring that all experimental data is included and decay data is up-to-date (collaboration with Brookhaven National Laboratory), including templates of experimental uncertainties [4], and further R-value validation calculations.

### References:

- [1] S. Okumura, Toshihiko Kawano, Patrick Talou, et al., *J. Nucl. Sci. Tech.* **55** (2018) 1009.
- [2] A.E. Lovell, T. Kawano, S. Okumura, et al., *Phys. Rev. C* **103** (2021) 014615.
- [3] M.B. Chadwick, T. Kawano, D.W. Barr, et al., *Nucl. Data Sheets* **111** (2010) 2923.
- [4] D. Neudecker, A.M. Lewis, E.F. Matthews, J. Vanhoy, et al., *EPJ Nucl. Sci. Technol.* **9**, 35 (2023).

## Q & A, Comments (C)

Q: What about the  $^{235}\text{U}$  delayed neutron energy dependence by Obninsk?

A: We have energy dependence of delayed neutrons too.

C: Some data at thermal should be better reproduced.

A: Yes, fine tuning is ongoing.

### 2.19 Preliminary study on photo-nuclear fission product yield evaluation, T. Kawano

Prompt and beta-delayed fission observables, such as the average number of prompt and delayed neutrons and photons, the independent and cumulative fission product yields, and the prompt neutron and gamma-ray energy spectra for the photonuclear reactions on  $^{235,238}\text{U}$  and  $^{239}\text{Pu}$  were calculated with the Hauser-Feshbach Fission Fragment Decay (HF3D) model implemented on the CoH3/BeOH codes, where the model parameters were inferred by the neutron-induced fission cases. For the prompt fission gamma-ray production data, we adopted a finer energy grid to keep all the discrete gamma-line structures.

By applying neutron-induced fission reactions to the case of photo-induced fission, an excellent reproduction of the delayed neutron yields supports the traditional assumption that the photo-fission might be similar to the neutron-induced fission at the same excitation energies, regardless of the spin and parity of the fissioning systems. This was published in [1].

This procedure produced the evaluated independent and cumulative fission product yields from 1 to 25 MeV. Comparisons with the HIgS experimental at 13 MeV and the bremsstrahlung data at 25 MeV look reasonable. However, we still plan to perform fine-tuning of model parameters based on Lovell's new FPY evaluations for neutron-induced fission.

#### References:

[1] T. Kawano, A.E. Lovell, S. Okumura, et al., Phys. Rev. C107 (2023) 044608.

### 2.20 Verification of the energy dependence of the fission product yields from the GEF code for neutron induced fission of $^{235}\text{U}$ based on delayed neutron temporal data, V.M. Piksaikin

Co-authors: K.V. Mitrofanov, A.S. Egorov, D.E. Gremyachkin, V.F. Mitrofanov, State Scientific Center of the Russian Federation Institute of Physics and Power Engineering Obninsk, Russia

Because this talk was presented by P. Dimitriou, who was not an author of the study, there was no discussion.

#### 2.20.1 Introduction

The energy dependence of delayed neutron (DN) macroscopic data in the energy range higher than 5 MeV still needs to be carefully investigated. The data on the relative abundances and the half-lives of delayed neutron precursors from fission of  $^{235}\text{U}$  in this energy range are presented in the paper by Maksyutenko et al. [1]. These data are not consistent with the energy dependence of the average half-life  $\langle T_{1/2}(E_n) \rangle$  of DN precursors which can be estimated employing,

$$\langle T_{1/2}(A, E_n) \rangle = \frac{\sigma_{n,f1} \cdot \langle T_{1/2}(A, E_n) \rangle + \sigma_{n,n'f} \cdot \langle T_{1/2}(A-1, E_{n1}) \rangle}{\sigma_f(E_n)}, \quad (1)$$

where  $\sigma_f(E_n) = \sigma_{n,f1} + \sigma_{n,n'f}$ ,  $\sigma_{n,f1}$ ,  $\sigma_{n,n'f}$ , is the total fission cross section (the sum of all

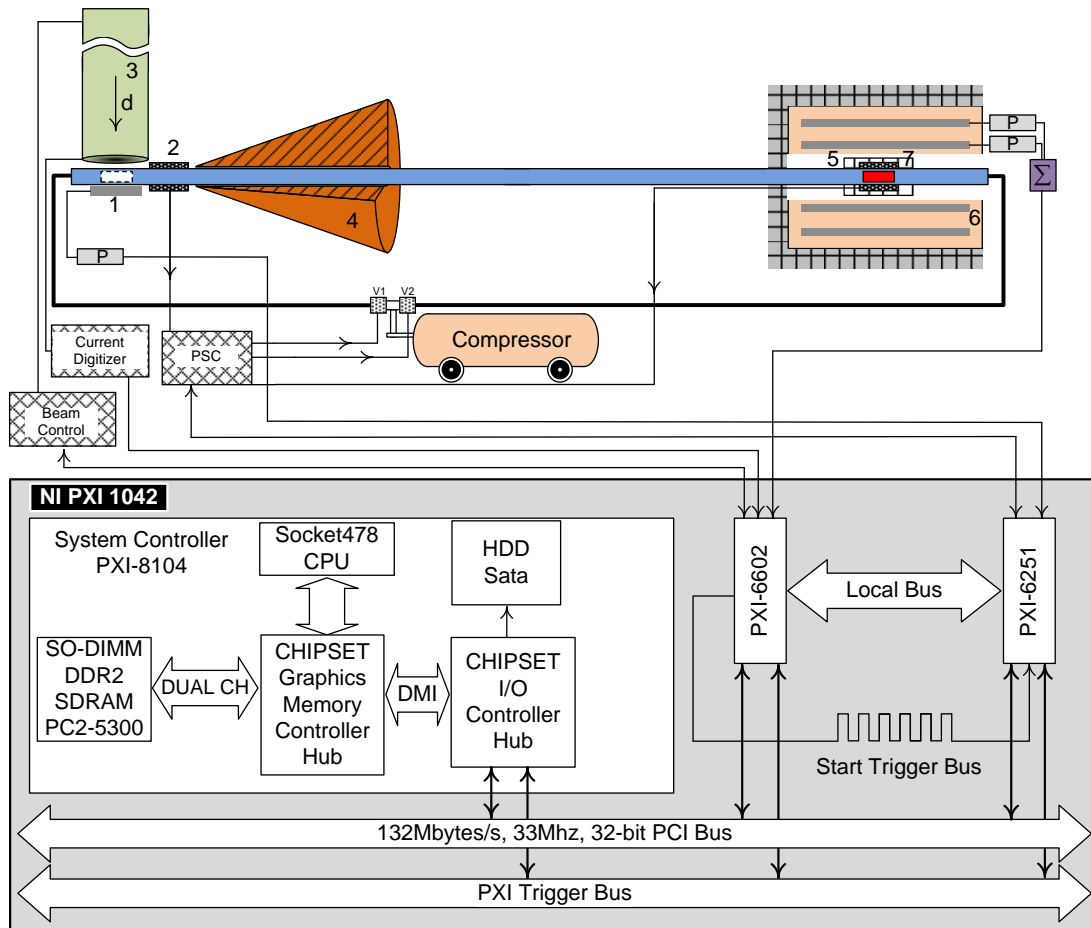
chances), the first and second chance fission cross sections, respectively, and  $A$  is the atomic number of the target nuclide. Calculations for the fission of  $^{235}\text{U}$  have been made using the fission cross section from ENDF/B-VII and  $\langle T_{1/2}(A-I) \rangle$  for  $^{234}\text{U}$  from systematics [2] and showed that  $\langle T_{1/2} \rangle$  at a neutron energy of 8 MeV was equal to 9.5 s. Thus  $\langle T_{1/2} \rangle$  in Maksyutenko et al., 12.5 s, is an overestimate by about 3 s.

The purpose of this work is to extend the energy range of data on the relative abundances and the periods of DN from fission of  $^{235}\text{U}$  beyond the threshold of the  $^{235}\text{U}(n,n'f)$  reaction. These data are important for reactor kinetic calculations as well as for the verification of the fission yield data [3] and the analyses of fission chances [4]. The measurements of the DN relative abundances and the half-lives of their precursors from neutron-induced fission of  $^{235}\text{U}$  in the energy range 0.4-8 MeV have been made on a modified experimental set-up of the IPPE. These data were used to verify the energy dependence of the  $^{235}\text{U}$  fission product yield data from GEF [5].

### 2.20.2 Experimental set-up

A new experimental set up was installed on the ion beam line of the electrostatic accelerator of the IPPE. The main components of the set up are shown in Fig.1.

FIG. 1. Experimental set up used to investigate DN characteristics.



P: preamplifier, amplifier, and discriminator unit;  $\Sigma$ : pulse summation module; V1 and V2: electromagnetic valves; PSC: pneumatic system control module; 1: fission chamber; 2 and 5: sample position detectors; 6: neutron detector; 4:  $4\pi$  neutron shielding, 7: shielding. The electronics used for acquisition, processing, and visual control of the measurement and accumulation of experimental data is based on the National Instruments (NI) modules described in the text.



A short description of some components of the set-up is presented below.

### 1. $4\pi$ -neutron detector

A cylindrical polyethylene block with a central channel for installing a pneumatic transport system and Pb shield was used as a moderator of registered neutrons. 21 proportional  $^3\text{He}$  counters were placed in the moderating matrix parallel to the central channel along two concentric circles. The main criteria for choosing the configuration of the  $^3\text{He}$ -counters in the matrix was the maximum neutron detection efficiency and the minimum energy dependence of the efficiency in the energy range corresponding to the DN energy spectrum.

The optimization of the placement of  $^3\text{He}$ -counters in the detector moderator was carried out by Monte Carlo simulations of various possible configurations. The variation in the radii of the two concentric rings of the  $^3\text{He}$ -counters  $R_1$  and  $R_2$  showed that when using a cylindrical moderator with a diameter of 50.5 cm and a height of 64 cm, the maximum detector efficiency with minimum energy dependence was achieved at  $R_1 = 10.9$  cm and  $R_2 = 14.9$  cm.

The energy dependence of the neutron detection efficiency is flat in the DN energy range with a value of close to 40%. The value of the efficiency  $\langle \varepsilon_n \rangle$ , weighted by the prompt neutron spectra of  $^{252}\text{Cf}$ , is  $\langle \varepsilon_n \rangle = 34.96 \pm 0.81\%$ .

### 2. Data acquisition system

The electronics for acquisition, processing, and visual control for measuring and accumulating the experimental data are based on National Instruments (NI) modules. The system includes a PXI-8104 controller, a PXI-6602 timer/counter, and a PXI-6251 multifunctional module. All modules are installed in a PXI-1042 rack (see Fig. 1), equipped with a PXI/PCI bus, allowing the controller processor and individual modules to be integrated into a single platform. The signals from the neutron detector were fed sequentially to preamplifiers, amplifiers, and discriminators. Registration of the number of pulses coming from the detectors to the data acquisition system was carried out continuously, including the time for irradiation of the sample and counting the DN activity after the interruption of the ion beam.

### 3. Neutron source

A monoenergetic neutron flux was generated by  $^7\text{Li}(p,n)^7\text{Be}$  and  $\text{D}(d,n)^3\text{He}$  reactions in the neutron energy ranges 0.42 – 2.92 MeV and 4 - 8 MeV, respectively. The proton and deuteron beams at the appropriate energy were provided by the 6 MeV electrostatic accelerator at the IPPE. Lithium targets were prepared by evaporating LiF onto 0.5 mm copper backings. Deuterium targets were made from deuterium absorbed in a  $\sim 1$  mg/cm<sup>2</sup> thick Ti layer deposited on 0.5 mm copper backings. The target thicknesses were chosen so that ion energy loss in the target did not exceed the neutron kinematic energy spread.

The neutron energy distribution from the  $\text{D}(d,n)^3\text{He}$  reaction,  $d^2N(\theta, E_n)/(d\Omega \cdot dE_n)$ , at  $0^\circ$  with respect to the deuteron, for neutron energies of 1 to 5 MeV were measured using a spectrometer based on stilbene crystals. The spectrometer was placed to shield against neutrons scattered in the experimental hall. The gamma background was suppressed by a lead sheet filter. The spectrometer energy scale was calibrated using standard  $^{137}\text{Cs}$  and  $^{60}\text{Co}$  gamma sources. A correction was introduced for the transmission function of the lead filter, calculated using a Monte Carlo simulation. The measured spectra from the  $\text{D}(d,n)^3\text{He}$  reaction on the D-Ti target emitted at  $0^\circ$  are shown in Fig.2.

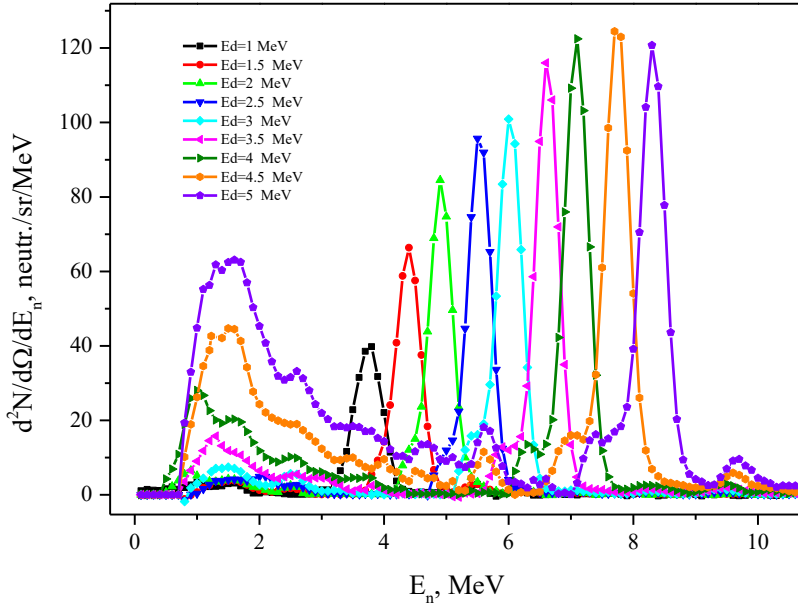


FIG. 2. The energy spectra of neutrons  $d^2N(\theta, E_n) / (d\Omega \cdot dE_n)$  from the  $D(d,n)^3\text{He}$  reaction on a D-Ti target at  $\theta = 0^\circ$  relative to the deuteron beam, measured with a spectrometer using stilbene crystals (normalized on one incident deuteron).

It can be seen from Fig. 2 that the low-energy neutron component is observed even for deuteron energies of 3.5 MeV. At 4.5 MeV the neutron contribution likely due to the break-up reaction  $\text{Cu}(d,pn)\text{Cu}$  becomes comparable to the neutron component of  $D(d,n)^3\text{He}$  and, by 5 MeV, it is twice as high. The integral of the spectra  $\int (d^2N(\theta, E_n) / d\Omega \cdot dE_n) dE_n$  in the energy range of break-up neutrons and in the range of monoenergetic neutrons makes it possible to separate the differential cross sections of the main component from the  $D(d,n)^3\text{He}$  reaction (monoenergetic) and the break-up reaction  $\text{Cu}(d,pn)\text{Cu}$  (non-monoenergetic). The data are presented in Fig. 3. The differential cross section  $d\sigma(\theta) / d\Omega$  for the monoenergetic reaction at  $\theta = 0^\circ$  using the estimate of Drosg [6] is shown for comparison.

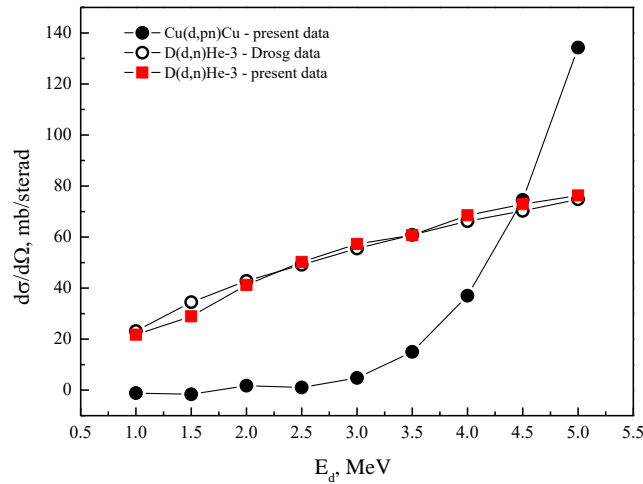


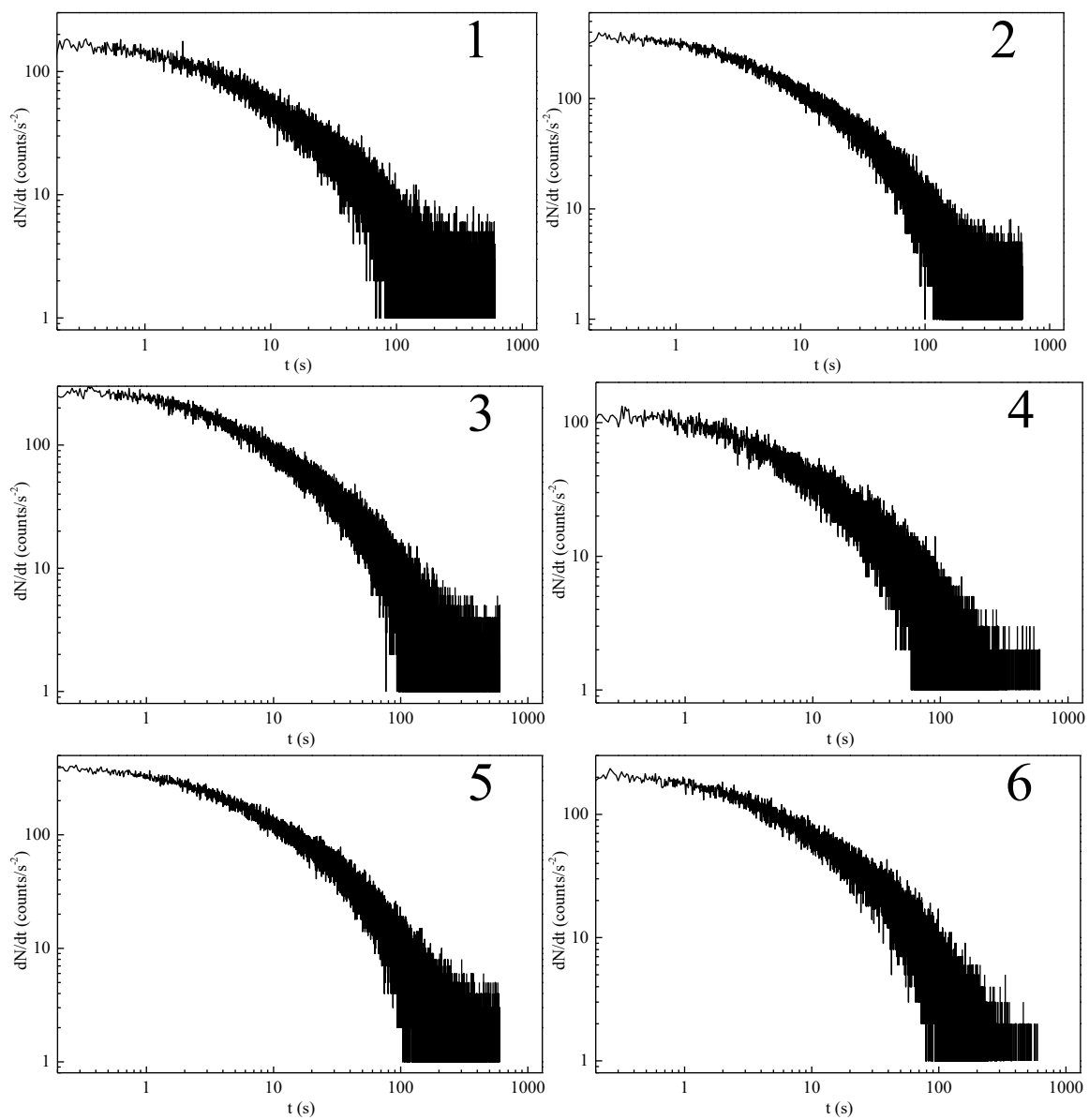
FIG. 3. The differential cross section  $d\sigma(\theta) / d\Omega$  from the primary monoenergetic  $D(d,n)^3\text{He}$  reaction and that of the break-up reaction  $\text{Cu}(d,pn)\text{Cu}$  (non-monoenergetic) at  $\theta = 0^\circ$ . The data from the monoenergetic reaction at  $\theta = 0^\circ$  using the estimate from Drosg [6] is shown for comparison.

The non-monoenergetic component of neutron spectrum is background accounted for when processing the experimental decay curves.

### 2.20.3 The measurement procedure and processing of the experimental data

The experimental method employed in these experiments is based on cyclic irradiations of the fissionable samples followed by the measurement of the time dependence of the delayed neutron activity. During irradiation, the ion current incident on the neutron target, the pulse spectra from the  $^{239}\text{Pu}$  fission chamber, and the neutron detector counts were registered. The neutron detector stability was checked every day by counting the Pu-Be source in a standard geometry. The irradiation time was 180 and 15 s. The DN counting time was 600 s for long irradiation and 500 s for short irradiation experiments. The sample delivery time in this experiment was about 200 ms.

The collected DN decay data curves were summed over all cycles and transformed in the time scale with a channel width of 0.01 s. Some of the transformed data measured in the  $\text{D}(d,n)^3\text{He}$  reaction are shown in Fig. 4.



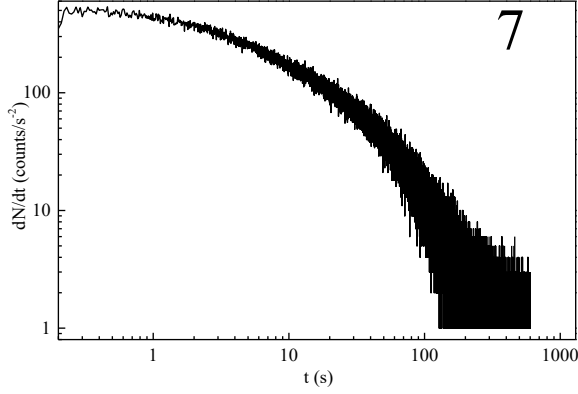


FIG. 4. DN decay curves from neutron-induced fission of  $^{235}\text{U}$  in the deuteron energy range 1-5 MeV in uniform scale in time bins of 0.01 s. 1:  $E_d = 1$  MeV,  $E_n = 4.15$  MeV, 82 irradiation cycles; 2:  $E_d = 2$  MeV,  $E_n = 5.25$  MeV, 74 cycles; 3:  $E_d = 3$  MeV,  $E_n = 6.27$  MeV, 35 cycles; 4:  $E_d = 3.5$  MeV,  $E_n = 6.77$  MeV, 9 cycles; 5:  $E_d = 4$  MeV,  $E_n = 27$  MeV, 22 cycles; 6:  $E_d = 4.5$  MeV,  $E_n = 7.76$  MeV, 5 cycles; 7:  $E_d = 5$  MeV,  $E_n = 8.25$  MeV, 12 cycles.

The analysis of the DN decay curves to estimate the relative abundances and DN periods employed the iterative least-squares procedure described in Ref. [7]. The equation used to model cyclic irradiation in the Least Square Method (LSM) is

$$N(t_k) = A \cdot \sum_{i=1}^m T_i \cdot \frac{a_i}{\lambda_i} \cdot (1 - e^{-\lambda_i \Delta t_k}) \cdot e^{-\lambda_i t_k} + B \cdot \Delta t_k, \quad (2)$$

$$T_i = (1 - e^{-\lambda_i t_{irr}}) \cdot \left( \frac{n}{1 - e^{-\lambda_i T}} - e^{-\lambda_i T} \cdot \left( \frac{1 - e^{-n \lambda_i T}}{(1 - e^{-\lambda_i T})^2} \right) \right), \quad A = \varepsilon_n \sigma_f \varphi N_f v_d,$$

where  $N(t_k)$  is the number of counts registered by the neutron detector in time channel  $t_k$  with width  $\Delta t_k$ ;  $v_d$  is the total DN yield per fission;  $B$  is the intensity of the neutron background;  $\lambda_i$  and  $a_i$  are the decay constant and the relative abundance of the  $i^{\text{th}}$  DN group;  $n$  is the number of cycles;  $m$  is the number of DN groups;  $T$  is the duration of one cycle of measurements, including the irradiation and the DN counting time;  $t_{ir}$  is the irradiation time,  $\varepsilon_n$  is the neutron detection efficiency;  $\varphi$  is the neutron flux;  $\sigma_f$  is the fission cross section; and  $N_f$  is the number of atoms in the sample under investigation.

The correction for break-up neutrons is

$$N(t_k) = N_{dn}(t_k) + N_{dpn}(t_k),$$

where  $N_{dn}$  is the decay curve of incident neutrons emitted from the primary reaction and  $N_{dpn}$  is the decay curve generated by break-up neutrons.  $N_{dpn}(t_k)$  was estimated using Eq. (2) with the average energy from the  $N_{dpn}$  spectra (see Fig. 2) and the corresponding DN parameters ( $a_i$ ,  $T_i$ ) measured using the  $^7\text{Li}(p,n)^7\text{Be}$  reaction.

#### 2.20.4 Results and discussion

The data on the energy dependence of the DN relative abundance and the half-lives of their precursors in neutron-induced fission of  $^{235}\text{U}$  are presented in the 6-group model. The data, obtained over several runs for specified energies of primary neutrons, were averaged, taking into account the correlation matrices calculated for each run [8].

A comparison between the present DN temporal data and data measured by previously is shown in Fig. 5 as a function of the average DN precursor half-life,

$$\langle T_{1/2} \rangle = \sum_{i=1}^6 T_i \cdot a_i$$

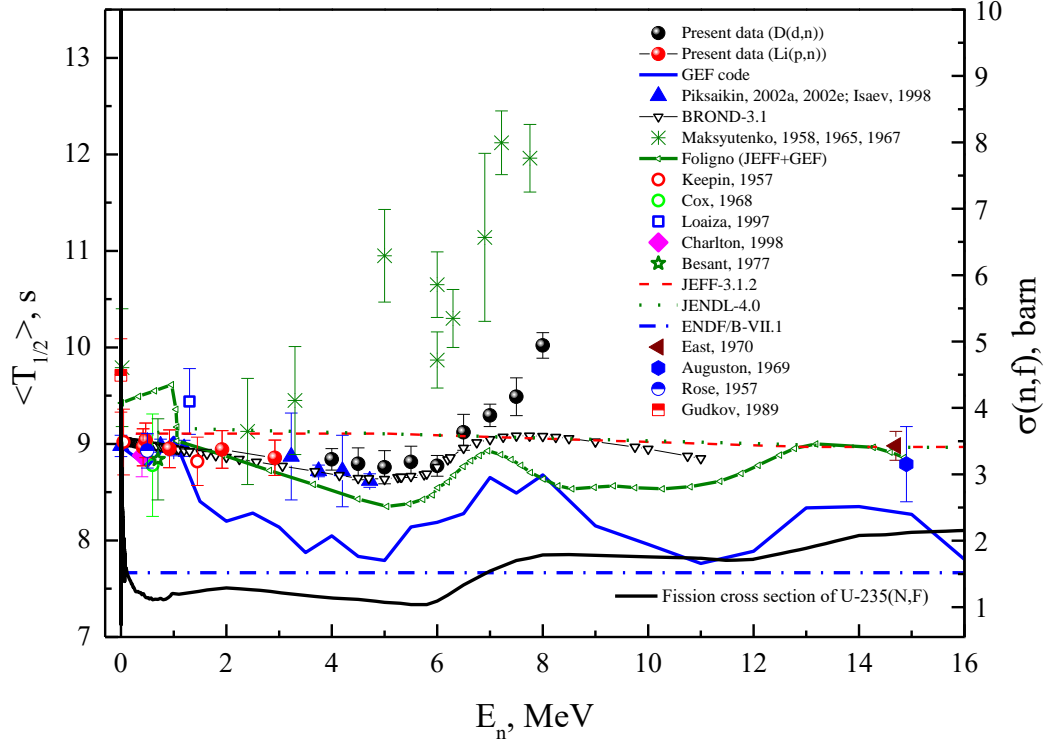


FIG. 5. The energy dependence of the average half-life of DN precursors from neutron-induced fission of  $^{235}\text{U}$ . The  $\langle T_{1/2} \rangle$  data for energies up to 4 MeV was obtained with the Li(p,n) reaction while, in the 4-8 MeV energy range, the D(d,n) reaction was used. The present data were corrected for the low energy component (LEC) of incident neutrons. References to previous data and evaluations can be found in Ref. [9]. The Foligno (JEFF+GEF) data are discussed in Ref. [10].

In Fig. 5, in addition to the experimental data, the energy dependence of the  $\langle T_{1/2} \rangle$  values was calculated using the summation method

$$\langle T_{1/2}(E_n) \rangle = \frac{\sum_i P_{ni} \cdot CY_i(E_n) \cdot T_{1/2,i}}{\sum_i P_{ni} \cdot CY_i(E_n)}, \quad (3)$$

where  $CY_i(E_n)$  is the cumulative yield of  $i^{\text{th}}$  DN precursor,  $P_{ni}$  and  $T_{1/2,i}$  is the DN emission probability and the half-life of  $i^{\text{th}}$  precursor, respectively. The cumulative yields of delayed neutron precursors  $CY_i(E_n)$  were obtained using the GEF code [6]. The summation was made over all precursors included in the new microscopic database from an IAEA CRP [11].

Figure 5 shows that the present dependence of  $\langle T_{1/2}(E_n) \rangle$  agrees within uncertainties with the dependence obtained earlier by the authors in the energy range from thermal to 5 MeV. The discrepancies with the Maksyutenko et al. data were discussed in the introduction. The most probable reason for these discrepancies is the “blocking” effect [12] because the neutron detector was placed in the vicinity of the neutron target since there was no rabbit system for the transportation of the sample.

The most important features of these data are the smooth decrease of  $\langle T_{1/2}(E_n) \rangle$  in the energy range from thermal to ~6 MeV and a steeper increase in the energy range above the second chance fission threshold. The data on  $\langle T_{1/2}(E_n) \rangle$  obtained with the fission yields  $CY_i(E_n)$  from the GEF code agrees with the present data in the energy range from thermal to 1 MeV. In this energy range there are many fission fragment yield data that provide a good basis for determining the GEF model parameters. In the region above 1 MeV the GEF-based  $\langle T_{1/2}(E_n) \rangle$  data reproduce the general trend observed in our data but lie systematically below them with  $\Delta \langle T_{1/2} \rangle \approx 1$  s. The most probable reason for this discrepancy is an underestimate of the cumulative yields above 1 MeV in the GEF code because the

microscopic DN data ( $P_{ni}$ ,  $T_{1/2,i}$ ) used to calculate  $\langle T_{1/2}(E_n) \rangle$  values are held fixed over the entire energy range. The low fission product yields can be related to the estimate of the most probable charge of isobaric beta-decay chains.

The energy dependence of  $\langle T_{1/2}(E_n) \rangle$  can be estimated based on the chance structure of the fission cross section of  $^{235}\text{U}$  using Eq. (1). The cross sections for first and second chance fission were taken from ENDF/B-VII.I. These data on  $\langle T_{1/2}(E_n) \rangle$  were used for first chance fission,  $\sigma_{n,f1}(E_n)$  ( $n+^{235}\text{U}$ ). The values of  $\langle T_{1/2}(E_n) \rangle$  for second chance fission,  $\sigma_{n,n}(E_n)$  ( $n+^{234}\text{U}$ ), were estimated employing systematics [2]. Figure 5 shows that the energy dependence of  $\langle T_{1/2}(E_n) \rangle$  estimated by GEF changes slope (from decreasing to increasing) at the same energy where this change occurs in the present data.

#### References:

- [1] B.P. Maksyutenko, et al., Relative yields of delayed neutrons in fission of  $^{238}\text{U}$ ,  $^{235}\text{U}$  and  $^{232}\text{Th}$  by fast neutrons, J. Exptl. Theor. Phys. (USSR) **35** (1958) 815.
- [2] V.M. Piksaikin, S.G. Isaev, and A.A. Goverdovski, Characteristics of Delayed Neutrons: Systematics and Correlation Properties, Prog. Nucl. Energy **41**, Issues 1-4 (2002) 361-384.
- [3] D.E. Gremyachkin, V.M. Piksaikin, K.V. Mitrofanov, and A.S. Egorov, Verification of the evaluated fission product yields data from the neutron induced fission of  $^{235}\text{U}$ ,  $^{238}\text{U}$  and  $^{239}\text{Pu}$  based on the delayed neutron characteristics, Prog. Nucl. Energy **83** (2015) 13-25.
- [4] D.E. Gremyachkin, V.M. Piksaikin, A.S. Egorov, V.F. Mitrofanov, and K.V. Mitrofanov, Investigation of the chance structure of the fission cross section of  $^{238}\text{U}$  by neutrons in the energy range from 14 to 18 MeV using the delayed neutrons, Prog. Nucl. Energy **118** (2020) 103068.
- [5] GEF – A General description of the Fission process.  
URL: <https://www.lp2ib.in2p3.fr/nucleaire/nex/gef/>
- [6] DROSG-2000: Neutron Source Reactions. Data files with Computer codes for 60 accelerator-based neutron source reactions prepared by M. Drogg, Faculty of Physics, University of Vienna, Austria Version 12.01 (March 2017).  
URL: <https://www-nds.iaea.org/public/libraries/drogsg2000/>
- [7] V.M. Piksaikin, L.E. Kazakov, S.G. Isaev, M.Z. Tarasko, V.A. Roshchenko, R.G. Tertytchnyi, G.D. Spriggs, and J.M. Campbell, Energy dependence of relative abundances and periods of delayed neutrons from neutron-induced fission of  $^{235}\text{U}$ ,  $^{238}\text{U}$ ,  $^{239}\text{Pu}$  in 6- and 8-group model representation, Prog. Nucl. Energy **41**, Issues 1-4 (2002) 203-222.
- [8] V.M. Piksaikin, A.S. Egorov, D.E. Gremyachkin, K.V. Mitrofanov, V.F. Mitrofanov, Generation of correlation and covariance matrices for the recommended temporal DN parameters in 6- and 8-group models, EPJ Nuclear Sci. Technol. **6** (2020) 54.  
URL: <https://doi.org/10.1051/epjn/2020013>
- [9] G.D. Spriggs and J.M. Campbell, A Summary of measured delayed neutron group parameters, Prog. Nucl. Energy **41**, Issues 1-4 (2002) 145-201.
- [10] D. Foligno, New evaluation of delayed-neutron data and associated covariances. PhD thesis, Université Aix-Marseille (2019).
- [11] P. Dimitriou, I. Dillmann, B. Singh, et al, Development of a Reference Database for Beta-Delayed Neutron Emission, Nuclr Data Sheets **173** (2021) 144-238. Reference Database for Beta-Delayed Neutron Emission: <https://www-nds.iaea.org/beta-delayed-neutron/database.html>
- [12] V.M. Piksaikin, V.A. Roshchenko, G.G. Korolev. Relative Abundances of Delayed Neutrons and Half-lives of Their Precursors from Neutron Induced Fission of  $^{238}\text{U}$  in the Incident Neutron Energy Range 14.2–17.9 MeV, Atomic Energy V.102 №2 (2007)129-132 (in Russian).

## 2.21 Benchmarking fission yields with beta decay data (and vice versa), A. Algora

For the Valencia-Nantes collaboration

An overview of total absorption measurements of beta decays relevant for reactor applications, performed by the Valencia-Nantes collaboration at the University of Jyväskylä IGISOL facility, were presented. The main goal of the work has been to identify the most relevant beta decays impacting these applications and measure them with the total absorption technique [1], a technique that provides

beta decay data free from the Pandemonium effect [2]. Some representative cases were shown [3, 4] and new developments in experimental and analysis techniques were presented, including an improved method for the determination of the ground state to ground state beta decay feedings [5]. The impact of the measurements in decay heat summation calculations for the  $^{235}\text{U}$  and  $^{239}\text{Pu}$  fuels (Fig. 1) [1, 6], as well as the results from recent summation calculations of the antineutrino spectrum in reactors compared to the DAYA BAY measurements, were shown (Figs 2 and 3) [7]. The importance of the decay data for constraining fission yields in these applications was discussed. Possible contributions of the Nantes-Valencia collaboration to this CRP were presented.

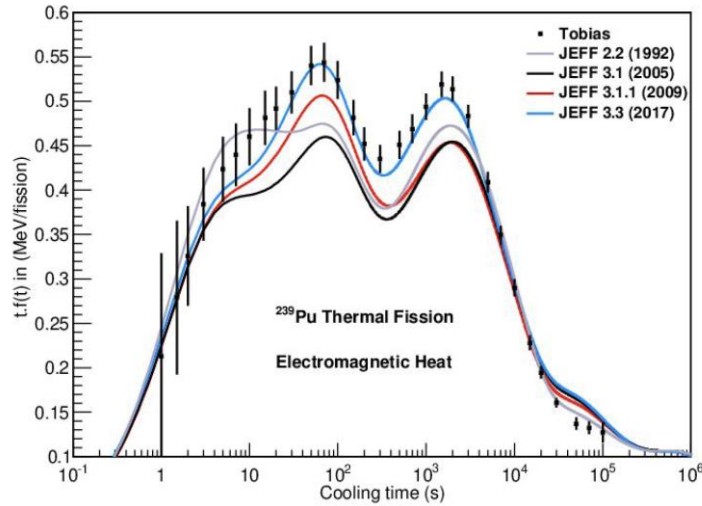


FIG 1. Comparison of the gamma component of the  $^{239}\text{Pu}$  decay heat (thermal fission) with summation calculations using different versions of the JEFF library [6].

Figure 1 shows the impact of the decay and fission yield data considered in the different versions of the JEFF library with a notable improvement depending on the included TAGS data. Experimental data is taken from the Tobias compilation.

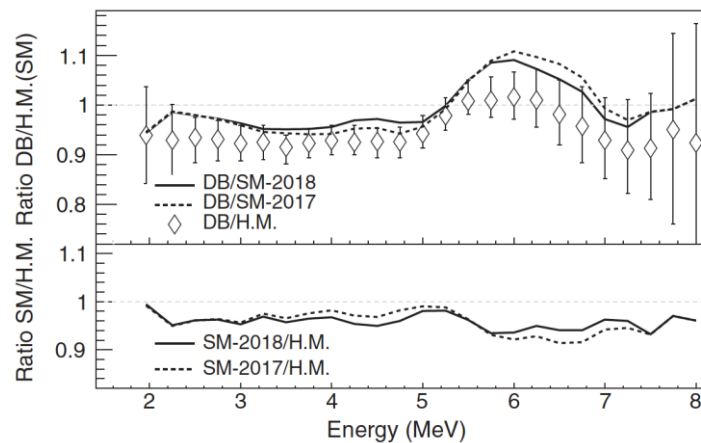


FIG. 2. Comparison of the ratio of the DAYA BAY neutrino flux (DB) with the predictions of the different models (H.M.: Huber-Mueller; SM-2017, SM-2018: summation models from years 2017 and 2018).

The Huber-Mueller model is considered the standard of the field. The summation models SM-2017, and SM-2018 differ on the amount of TAGS data included (for more details see [7].)

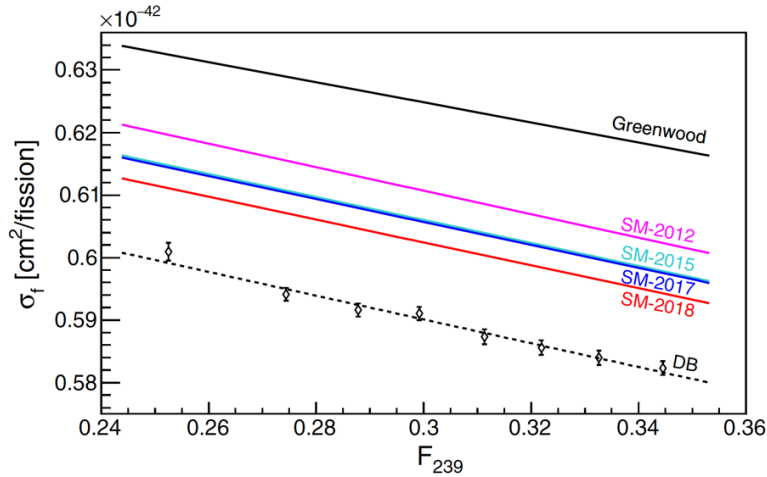


FIG. 3. Comparison of the inverse beta decay yield (IBD) of the DAYA BAY experiment as a function of the  $^{239}\text{Pu}$  fission fraction with the predictions of the different antineutrino summation models.

The summation models differ on the TAGS data included (represented in Fig. 3 by the year 20XY of the summation model SM-20XY). The agreement with the experimental data notably improved by adding more TAGS data, therefore, questioning the reactor anomaly (for more details see [7]).

#### References:

- [1] A. Algora, J.L. Tain, B. Rubio, et al., Eur. Phys. J. A **57**, 85 (2021).
- [2] J.C. Hardy, L.C. Carraz, P.G. Hansen, et al., Phys. Lett. B **71** (1977) 307.
- [3] V. Guadilla, A. Algora, J.L. Tain, et al., Phys. Rev. Lett. **122** (2019) 042502.
- [4] A.A. Zakari-Issoufou, M. Fallot, A. Porta, et al., Phys. Rev. Lett. **115** (2015) 102503.
- [5] V. Guadilla, J.L. Tain, A. Algora, et al., Phys. Rev. C **102** (2020) 064304.
- [6] A. Nichols, P. Dimitriou, A. Algora, et al., Eur. Phys. J. A **59**, 78 (2023).
- [7] M. Estienne, M. Fallot, A. Algora, et al., Phys. Rev. Lett. **123** (2019) 022502.

#### Q & A, Comments (C)

Q (S. Chiba): How does this compare with data? One should not be comparing to antineutrino data without comparing to yields as well.

C (R. Mills): Some issues can be raised with larger uncertainties, especially when there are fewer data available.

A: (Fallot) The best beta shape agreement is with  $^{235}\text{U}$  but the normalization doesn't match.

C (A. Algora): In the summation calculations always the commonly accepted yield evaluation was used, but clearly there is an impact of the selected yield data.

C (R. Capote): Validation is important.

A: (M. Fallot): If one fixes the decay data, it is possible to compare the effects of different sets of fission yields.

C (R. Mills): One needs to be careful about what decay data are being used for. They may not be good representations of beta transitions for many isotopes. Some improvements in agreement with data may be harder to quantify due to decay data.

C (P. Dimitriou): Decay heat shows that decay data can be improved via TAGS and gamma ray spectroscopy and then compared to  $Y(A)$ . More and better decay data with uncertainties, along with good integral data, are needed to be able to draw conclusions.

Q (R. Capote): How can decay data be independently validated? Maybe with more data at energies above thermal?



## 2.22 Accuracy evaluation of available fission yield data and updating, N. Mohamed

Progress in the first year was built on calculations to evaluate the accuracy of fission yield data using benchmark nuclear reactors. They have been testing ENDF/B-VIII.0 (also ENDF/B-VII.1) and JEFF3.3 in MCNPX V2.7.0 and WIMS-5B/CITVAP, Monte Carlo and deterministic codes respectively. The tests involve reactor criticality sensitivity to the accuracy of data libraries and criticality benchmarks used for evaluations.

Two research reactors were used for validation. ETRR-2 is modelled using deterministic codes while OPAL is modelled using Monte Carlo methods. Each reactor and method were evaluated separately because of cross section differences in each code. Fresh fuel is calculated to get differences in cross sections and burn up to check fission yield effects.

The ETRR-2 reactor is a 22 MW light water moderated and cooled open pool reactor with 29 fuel elements with a Co irradiation device for  $^{60}\text{Co}$  production. In 2009 ETRR-2 was modified to 27 fuel elements for LEU irradiation for  $^{99}\text{Mo}$  production. The studies used WIMS/CITVAP for modelling. WIMS is a general lattice cell code that solves neutron transport equation to calculation flux as a function of energy and position in cell. WIMS 5B has a 69-group data library with 14 fast groups above 9.118 keV and 42 thermal groups below 4 eV. The resonance range is covered by 13 groups. The result is spectrum dependent but also changes with temperature and geometry. CITVAP is a new version of the citation II code and solves diffusion transport for neutrons in one, two and three dimensions.

With the fresh core no fission products were generated. Starting with fresh core, good results were obtained with all three libraries. JEFF 3.3 has the best results, discrepancies are 100, 300 and 400 pcm for JEFF 3.3, ENDF/V-III.0, VII.1 respectively, acceptable. After 23 days of operation, errors increase to 800, 1000, and 1200 respectively for the same libraries while after 37 days from fresh core, errors were reduced to 400, 700 and 800 pcm respectively. These errors were large but deemed acceptable. They speculated that the errors could perhaps arise from the uncertainties in the fission yield data.

The OPAL reactor is compact core with a heavy water reflector, flat plate  $\text{U}_2\text{Si}_2\text{-Al}$  dispersion with Al cladding and 19.8 wt% of  $^{235}\text{U}$ , 2 Al side plates, each with 21 slots for 21 fuel plates and three types of fuel assembly. MCNPX 2.7.0 is used to calculate burnup with the same libraries.

The fresh core reactivity has smaller uncertainties, 25 pcm, than the deterministic calculations. The uncertainties increase somewhat with time but less than deterministic overall.

Progress in the second year was discussed next. The planned work relied on getting permission to irradiate natural  $\text{UO}_2$  at ETRR-2 to measure  $^{235}\text{U}$  fission yields.

Ten sub-samples of  $\text{UO}_2$  have been irradiated in the ETRR-2 research reactor. Samples were irradiated for short and long times: 30 sec for short and 15 min for flux monitors with 1 hour for long radiation. The irradiated samples have been measured using n-type HPGe detector at different decay times for quantifying the resulted fission products. Further analysis will be completed in the coming months.

## 2.23 Fission Yield data plotter at <https://nds.iaea.org/dataexplorer>, S. Okumura

The plotter provides data visualization for reaction and residual production cross sections and fission yields as a function of mass and isotope yield. It can show experimental and evaluated data and lists all data. While the default is set to the latest 20 experimental results, it is possible to search for older experimental data. It can retrieve the yields of primary fragments as well as independent and cumulative product yields. Users can zoom in on plots of the mass and charge yields as well as download files.

Data Explorer uses CSV tabulated format as data sources, converted and separated into single file in x-y form in a Fortran program. Python codes are used to read and plot files.

There are still some problems because EXFOR is not easy to use with data visualization software. They are working on improving the EXFOR interface with Data Explorer. It will be linked to a new EXFOR parser soon. It should also be possible to plot other fission observables.

#### **Q & A, Comments (C)**

Q (R. Mills): What is difference between C4 and C5?

A: C4 was based on what Red Cullen developed for cross sections while Zerkin developed C5 which can read more of EXFOR.

C (Koning): Reaction codes and subcodes have been developed over many years. Evaluators think of things differently and prefer to see measured (or evaluated) data formatted the same way and plotted together.

C (Kawano): EXFOR has expanded but he prefers to go to data files.

C (Chiba): He asked a postdoc to find all fission yield data in EXFOR. To do this the postdoc made a perl script to parse databases. They thought they had it all but found out that they had somehow missed important data.

### **3. RECOMMENDATIONS**

There followed some discussion of what the CRP would deliver. There will be 2 years until the next and final meeting (scheduled for 2-6 Dec 2024), followed by another year to produce the final publication, a journal paper. The goal is to produce a set of data together with documentation and the final article.

## APPENDIX 1

### 2nd Research Coordination Meeting on Updating Fission Yield Data for Applications

19 – 23 Dec 2022

IAEA, Vienna

Meeting Room MOE19 (virtual component)

#### ADOPTED AGENDA

**Monday, 19 December** (starting 13:00, open 12:45 Vienna time, 15:00 coffee break – 30min)

13:00	<b>Opening of the meeting, A. Koning / NDS Section Head</b>	
	<b>Election of Chair and Rapporteur(s), adoption of Agenda</b>	
	<b>Welcome and introduction, Roberto Capote Noy</b>	
13:30 – 17:30	<b>Participants' Presentations (~25' each, discussion as needed)</b>	
	O. Serot	Recent experimental fission yield results (non-exhaustive list, synthesis of the ND-2022 presentations)
	G. Kessedjian	New experimental data on $^{235}\text{U}(n_{\text{th}},f)$ mass yields performed on the Lohengrin mass spectrometer (preliminary results)
	I. Mardor T. Dickel	Preliminary results of $^{252}\text{Cf}$ spontaneous fission isotopic yields via mass measurements at the FRS Ion Catcher
	N. Shu	Progress in measurement of mass distribution of $^{235}\text{U}$ and $^{239}\text{Pu}$ fissions induced by Thermal Neutron at CNDC (Liu Shilong, Liu Chao)
	B. Prytichenko	Fission yield compilation status
	A. Tudora	Influence of energy partition in fission and pre-neutron fragment distributions on independent FPY ( $Y(Z, A_p)$ , $Y(A_p)$ ) and on kinetic energy distributions of post-neutron fragments. Correlation between the excitation energy of pre-neutron fragments and the kinetic energy of post-neutron fragments. Application for $^{235}\text{U}(n_{\text{th}},f)$ .

**Tuesday, 20 December** (starting 13:00, open 12:45 Vienna time, 15:00 coffee break – 30min)

13:00 - 17:30	<b>Participants' presentations: (~25' each, discussion as needed)</b>	
	F. Minato	Report on the result of the modelling subgroup, 15-20'
	N. Shu	Progress in theory and evaluation of fission yields at CNDC (Chen Yongjin, Liu Lile, Shu Nengchuan)
	S. Chiba	Developing the 4D-Langevin model-based fission fragment distribution database for TALYS
	A. Koning	Use of TALYS to calculate fission yields and neutron and gamma emission
	O. Serot	Impact of pre-neutron FY data on post-neutron FY by using the FIFRELIN de-excitation code
	J.-F. Lemaitre	Fission yields prediction with SPY & neutron evaporation with TALYS
	S. Hilaire	Microscopic determination of fission fragment distribution: current status
	R. Vogt	Generation of fission fragment angular momentum

19:30 Dinner in a restaurant (separate information)

**Wednesday, 21 December** (starting 13:00, open 12:45 Vienna time, 15:00 coffee break – 30min)

13:00 - 17:30	<b>Participants' presentations cont'd (~25' each, discussion as needed)</b>	
	R. Mills	Progress on UKFY3.7 development
	F. Minato	Evaluation of fission fragment yields and parameter optimization in CCONE code system
	G. Kessedjian	New methodology for FY evaluation (collaboration between NNL-CEA and Cadarache)
	G. Kessedjian	New $^{235}\text{U}(n_{\text{th}},f)$ fission yield evaluation and its validation (evaluation proposed for JEFF-4T2, collaboration between NNL and CEA-Cadarache)
	O. Serot	Preliminary results on $^{239}\text{Pu}(n_{\text{th}},f)$ mass yield evaluation
	A. Lovell	The ENDF Re-evaluation of Fission Product Yields
	T. Kawano	Preliminary study on photo-nuclear fission product yield evaluation.

**Thursday, 22 December** (starting 13:00, open 12:45 Vienna time, 15:00 coffee break – 30min)













13:00 - 17:30	<b>Participants' presentations cont'd (~20' each, discussion as needed)</b>	
	P. Dimitriou (V. Piksaikin)	Verification of the energy dependence of the fission product yields from the GEF code for neutron induced fission of $^{235}\text{U}$ based on delayed neutron temporary data
	A. Algora	Benchmarking fission yields with beta decay data (and vice versa)
	N. Mohamed	Accuracy evaluation of available fission yield data and updating
<b>Technical Discussions &amp; drafting of the meeting summary report</b>		







**Friday, 23 December** (starting 13:00, open 12:45 Vienna time)

13:00 - 15:00	<b>Technical Discussions &amp; drafting of the meeting summary report cont'</b>	
	<b>Closing of the meeting</b>	

## APPENDIX 2

### LIST OF PARTICIPANTS

Country		Name	Surname	Affiliation	Email
<b>CHINA</b>		Nengchuan	SHU	China Institute of Atomic Energy	nchshu@qq.com
<b>EGYPT</b>		Nader	MOHAMED	Egyptian Atomic Energy Authority	mnader73@yahoo.com
<b>FRANCE</b>		Olivier	SEROT	CEA-Cadarache	olivier.serot@cea.fr
		Gregoire	KESSEDJIAN	CEA-Cadarache	gregoire.kessedjian@cea.fr
		Muriel	FALLOT	Laboratoire Subatech, CNRS,in2p3	muriel.fallot@subatech.in2p3.fr
		Stephane	HILAIRE	CEA, DAM, DIF	stephane.hilaire@cea.fr
		Jean-Francois	LEMAITRE	CEA, DAM, DIF	jean-francois.lemaitre@cea.fr
<b>GERMANY</b>		Timo	DICKEL	GSI Helmholtzzentrum für Schwerionenforschung GmbH	t.dickel@gsi.de
<b>ISRAEL</b>		Israel	MARDOR	SOREQ, Israel Atomic Energy Commission	mardor@tauex.tau.ac.il
<b>JAPAN</b>		Satoshi	CHIBA	Tokyo Institute of Technology	chiba.s.ae@m.titech.ac.jp
		Futoshi	MINATO	Kyushu University	minato.futoshi@phys.kyushu-u.ac.jp
<b>ROMANIA</b>		Anabella	TUDORA	Bucharest University	anabellatudora@hotmail.com
<b>SPAIN</b>		Oscar	CABELLOS	Universidad Politecnica de Madrid	oscar.cabellos@upm.es
		Alejandro	ALGORA	CSIC-Universidad de València	algora@ific.uv.es
<b>SWEDEN</b>		Ali	EL-ADILI	Uppsala University	ali.al-adili@physics.uu.se

<b>SWITZERLAND</b>		Dimitri	ROCHMAN	Paul Scherrer Institut	dimitri-alexandre.rochman@psi
<b>UNITED KINGDOM</b>		Robert	MILLS	National Nuclear Laboratory Limited	robert.w.mills@uknnl.com
<b>USA</b>		Alejandro	SONZOGNI	Brookhaven National Laboratory	sonzogni@bnl.gov
		Toshihiko	KAWANO	Los Alamos National Laboratory	Kawano@lanl.gov
		Ramona	VOGT	Lawrence Livermore National Laboratory	rlvogt@lbl.gov
		Filip	KONDEV	Argonne National Laboratory	kondev@anl.gov
		Frederik	TOVESSON	Argonne National Laboratory	ftovesson@anl.gov
		Guy	SAVARD	Argonne National Laboratory	savard@anl.gov
<b>INT. ORGANIZATION</b>		Roberto	CAPOTE NOY	International Atomic Energy Agency	roberto.capotenoy@iaea.org
		Arjan	KONING	International Atomic Energy Agency	a.koning@iaea.org
		Paraskevi (Vivian)	DIMITRIOU	International Atomic Energy Agency	p.dimitriou@iaea.org
		Naohiko	OTSUKA	International Atomic Energy Agency	n.otsuka@iaea.org
		Shin	OKUMURA	International Atomic Energy Agency	s.okumura@iaea.org
		Georg	SCHNABEL	International Atomic Energy Agency	g.schnabel@iaea.org

## APPENDIX 3

### Meeting Photo – Online participants



### Meeting Photo – Participants present



---

Nuclear Data Section  
International Atomic Energy Agency  
Vienna International Centre, P.O. Box 100  
A-1400 Vienna, Austria

E-mail: [nds.contact-point@iaea.org](mailto:nds.contact-point@iaea.org)  
Fax: (43-1) 26007  
Telephone: (43-1) 2600 21725  
Web: <http://nds.iaea.org>

---